Trypanosome morphogenesis involves recruitment of a pleckstrin homology domain protein by an orphan kinesin to the microtubule quartet

Corinna Benz[1], Nora Müller[2], Marie Vancová[1,2], Sabine Kaltenbrunner[1,2,†], Hana Váchová[3], Vladimír Varga[3], Julius Lukeš[1,2], Hassan Hashimi[1,2,*]

[1]Institute of Parasitology, Biology Center, Czech Academy of Sciences, České Budějovice, Czechia

[2] Faculty of Science, University of South Bohemia, České Budějovice, Czechia

[3]Laboratory of Cell Motility, Institute of Molecular Genetics of the Czech Academy of Sciences, Prague, Czechia

[†]Current address: Johannes Kepler University, Medical Faculty, Linz, Austria

*Corresponding author: hassan@paru.cas.cz

Running title: TbKifX2 and TbPH1 association with the trypanosomal microtubule quartet

ABSTRACT

Kinesins are motor proteins found in all eukaryotic lineages that move along microtubule tracks to mediate numerous cellular processes such as mitosis and intracellular transport of cargo. In trypanosomatids, the kinesin protein superfamily has undergone a prominent expansion, giving these protists one of the most diverse kinesin repertoires. This has led to the emergence of two trypanosomatid-restricted groups of kinesins. Here, we characterize in *Trypanosoma brucei* TbKifX2, a hitherto orphaned kinesin that belongs to one of these groups. Representing a rare instance, TbKifX2 tightly interacts with TbPH1, a kinesin-like protein with an inactive motor domain. TbPH1 is named after a pleckstrin homology (PH) domain present within its carboxy-terminal tail. TbKifX2 recruits TbPH1 to the microtubule quartet (MtQ), a characteristic but poorly understood cytoskeletal structure that is part of the multipartite flagellum attachment zone (FAZ) and extends from the basal body to the anterior of the cell body. The proximal proteome of TbPH1 is comprised of four proteins that localize to the FAZ, consistent with the notion that the TbKifX2/TbPH1 complex are the first identified proteins to bind the MtQ along its whole length. Simultaneous ablation of both TbKifX2 and TbPH1 leads to the formation of prominent protrusions from the cell posterior. Thus, these two trypanosomatid-restricted proteins, which specifically localize to the MtQ in a microtubule-rich cell, appear to be contributors to morphogenesis in *T. brucei*.

IMPORTANCE

Trypanosomatids are a group of unicellular parasites that infect a wide range of hosts from land plants to animals. They are also eukaryotes that have been shaped by prolonged independent evolution since this domain of life has radiated from a common ancestor almost 2 billion years ago. Thus, any resulting unique biological properties can be potentially exploited for treatment of infectious diseases caused by trypanosomatids. The cytoskeleton of trypanosomatids represents an ancient organelle that has undergone such modification. Here, we show that two trypanosomatid-specific proteins named TbPH1 and TbKifX2 form a complex that localizes to the microtubule quartet, a cytoskeletal structure characteristic to trypanosomatids. Ablation of these proteins in *Trypansoma brucei* leads to distinct morphological defects, making them not only intrinsically interesting topics of study, but potential therapeutic targets as well.

INTRODUCTION

The vermiform morphology of the unicellular parasite *Trypanosoma brucei* that causes African trypanosomiasis in humans and nagana in cattle is defined by a subpellicular array of microtubules (MTs) (1–3). These MTs follow the helical path of the cell and are cross-linked to each other and the plasma membrane via regularly spaced fibrils (4). A high order is maintained within the corset with the MT plus ends converging at the parasite's posterior end and the minus ends located at the anterior of the cell (3).

The only place where the continuity of the *T. brucei* MT array is interrupted is at the flagellar pocket, the deep invagination where the flagellum exits the cell body and the only place where endo- and exocytoses occur (5). The opening of the flagellar pocket is encircled by a collar, which influences the overall shape of this cavity. Distal to the collar, the so-called hook complex covers the flagellum as it exits the flagellar pocket, with two lateral arms also flanking the flagellum attachment zone (FAZ) filament and the MT quartet (MtQ) inside the cell (6). The FAZ filament and MtQ are among the interconnected fibres, filaments and junctional complexes of the multipartite FAZ (7), which together form a lateral attachment for the flagellum as it follows a helical path along the cell body, connecting the flagellar skeleton to the cytoskeleton through both the flagellar and plasma membranes (8). The MtQ originates close to the basal bodies, wraps itself around the flagellar pocket and interdigitates within the MT corset next to the FAZ filament. The orientation of MTs in the MtQ is antiparallel to the one found within the MT corset, thus their minus ends are proximal to the basal bodies (3).

The trypanosome MT corset is exceptionally stable and only reorganised during cell division and life cycle transitions (9). All cytoskeletal structures (MtQ, MT corset, flagellum, basal bodies, which anchor the flagella within the cell, and FAZ) need to be duplicated and faithfully segregated during the cell division cycle, just like other single-copy organelles. In addition, this has to be coordinated with replication and division of the nucleus and the single mitochondrial DNA network termed the kinetoplast, which is located on the opposite side of the basal bodies relative to the flagellum (3, 10).

Basal body duplication and segregation are the first visible steps in the cell division cycle and essential for subsequent cytokinesis (11). The new MtQ starts growing just prior to basal body maturation and once the new flagellum has grown enough to invade the flagellar pocket, morphogenetic changes result in two separate pockets enveloping both the new and old flagella (12). New corset MTs are nucleated from the side of the existing ones and elongate on both the plus and minus ends during array replication (4). Once the new flagellum has been nucleated and

elongated, new MTs are integrated into the array between the old and new flagella, thereby increasing the overall width of the cell (1).

With its antiparallel orientation, the MtQ together with the FAZ filament create an asymmetric seam within the MT corset, which works as a cellular ruler and helps to determine the site of future furrow ingression during cytokinesis (8). Any insults to the integrity of these structures result in cytokinesis defects and it is thus tempting to envision the MtQ as a potential specialised “highway” in charge of transport and delivery of cargo to the site of important cytokinesis events. Furthermore, the endplasmic reticulum associates with parts of the MtQ, although the upshot of this association remains mysterious. The first protein localized to this structure, TbSpef1, is found at the proximal end of the MtQ, between basal bodies and the flagellar pocket collar (13). Its depletion causes problems with the biogenesis of the MtQ and associated structures as well as motility defects. The minus end of the MtQ MTs is anchored to the basal bodies by a protein named TbSAF1, found in close proximity to TbSpef1 but localized between the pro and mature basal bodies (14). TbSAF1 was found in a proximal proteomics screen of proteins adjoining to and/or directly interacting with TbSpef1 (*i.e.* the TbSpef1 proxisome), which found three additional proteins that localize to the MtQ between the basal body and flagellar pocket collar (14). However, no proteins that localise along the total length of the MtQ have thus far been identified nor have any motor proteins that may potentially bring cargo to the cytokinesis site.

Kinesins are well-studied motor proteins that regulate MT dynamics, organize MT networks, and transport cargo along MTs. Transporting kinesins can form homo- and heterodimers and consist of a head region containing the kinesin motor domain, which is responsible for ATP hydrolysis and MT binding, and a tail region important for dimerization with a kinesin/kinesin-like partner and cargo binding (15). In trypanosomatid genomes, kinesins and kinesin-like proteins constitute one of the largest protein superfamilies (16–18). To date, 47 genes encoding high-likelihood kinesins have been identified in the *T. brucei* genome (19, 20). Moreover, there is a similar number of kinesin-related proteins, which did not make the threshold due to sequence variance (16). Interestingly, numerous kinesins are members of two major clades named X-1 and X-2 that are restricted to the trypanosomatid lineage (19, 20). Why the kinesin repertoire has expanded so prominently in trypanosomatids remains mysterious.

Hitherto studied kinesins of *T. brucei* have been shown to be important for various processes occurring in different cellular compartments. KinA and KinB are involved in cell cycle progression and localise to the central spindle during mitosis (21) while TbKif13-1 localizes either to the nucleus or the mitotic spindle, where it meditates chromosome segregation during mitosis (22). KinC and KinD are distributed throughout the cytoskeleton, where they are involved in subpellicular MT organization, basal body segregation and cytokinesis (23, 24).

Some kinesins are associated with the flagellum and adjacent FAZ. KIN2A and KIN2B are kinesins involved in intraflagellar transport (IFT), a process that directly affects flagellar biogenesis and in turn affects cell motility and cytokinesis (25, 26). The orphan kinesin KIN-E predominantly localises to the flagellar tip and is required for elongation of the new FAZ (27). Another orphan kinesin named KLIF initially localises to the tip of the new, elongating FAZ and associates with the old FAZ as the cytokinetic furrow ingresses towards the posterior end, thus mediating the final stages of cytokinesis (28). Other kinesins localising to specific cytoskeletal structures include FCP2/TbKinX1 and FCP4/TbKin15, which are found at the flagella connector (FC), a trypanosome-specific structure that connects the outgrowing new flagellum to the old one (29). Interestingly, FCP2/TbKinX1 belongs to kinesin clade X-1, one of the two trypanosomatid-restricted kinesin families (19, 20).

126 Here we present data on the localisation and function of two members of the kinesin superfamily,
127 TbKifX2 and TbPH1, with the former protein belonging to clade X-2. Functional characterization and
128 the unique localization of these kinesins further expands our knowledge on how these diverse and
129 dexterous proteins affect the biology of these extremely diverse and successful parasites.

130

131 **RESULTS**

132 **TbPH1 is a kinesin-like protein that fractionates with the *T. brucei* cytoskeleton**

133 TbPH1 (Tb927.3.2490) is a 110 kDa protein named after a C-terminal pleckstrin homology (PH)
134 domain, which is followed by a proximate homeodomain-like (HDL) fold and preceded by a coiled
135 coil (CC) domain (Fig. 1). The protein undergoes post-translational modifications, with
136 phosphorylation of a serine at the start of the HDL (30) and a methylarginine in the middle of the
137 primary structure (31). While TbPH1 has an N-terminal kinesin motor domain, two substitutions of
138 highly conserved amino acids within the Walker A motif (G93P and T/S95R) likely ablate the ATP
139 hydrolase activity. Thus, TbPH1 is unlikely to be a *bona fide* kinesin motor protein**.**

140 TbPH1 also belongs to the ~2000 proteins found in the granule-enriched fraction (containing cellular
141 aggregates, nuclei, kinetoplasts and flagella as well as associated cytoskeletal structures) obtained
142 by 'MT sieving', a method originally conceived to purify stress granules from *T. brucei* (32). In brief
143 (see S1 Fig. for 'MT sieving' pipeline), cells are lysed by non-ionic detergent in low ionic strength
144 buffer, which maintains the cytoskeleton, including the MT corset that in turn cages predominantly
145 detergent insoluble cellular structures with at least one dimension >20-30 nm. The cytoskeleton is
146 then disrupted by 300 mM NaCl to release these elements for subsequent analysis.

147 To verify TbPH1's apparent association with cytoskeletal fractions, we subjected a *T. brucei* cell line
148 in which the endogenous *TbPH1* open reading frame was appended with a C-terminal V5 tag (33) to
149 cell fractionation by a procedure identical to 'MT sieving'. The cell equivalents of the ensuing
150 fractions were inspected for the presence of TbPH1-V5 and SCD6, a stress granule marker that
151 served as a control for this method (Fig. 2A). SCD6 was mostly found in the soluble fractions as
152 previously reported for unstressed *T. brucei* (32), with a distribution across the analysed fractions
153 very distinct from that of TbPH1-V5. TbPH1-V5 was well retained in all cytoskeletal fractions P1 and
154 P2, although a fraction was released in the SN1 with other soluble cytosolic proteins upon initial lysis
155 (Fig. 2A). Importantly, indirect immunofluorescence (IFA) using an anti-V5 antibody on
156 formaldehyde-fixed P2 fraction shows that TbPH1-V5 is localized as a line extending from the DAPI-
157 stained kinetoplast (Fig. 2B) that decreases in signal intensity distally, suggestive of a cytoskeletal
158 localization. This was confirmed by the observation that the vast majority of TbPH1 was released
159 into the soluble SN3 fraction after high salt disintegration of the cytoskeleton. A small amount of
160 TbPH1-V5 was still found in the final pellet P3, which is consistent with its detection in the cohort of
161 proteins retained by 'MT sieving' (32). Thus, TbPH1 is a kinesin-like protein that fractionates with the
162 trypanosomal cytoskeleton.

163 **TbPH1 strongly interacts with the trypanosomatid-restricted orphan kinesin TbKifX2**

164 Because kinesins tend to form dimers (34) and kinesin-like TbPH1 contains a CC domain (Fig. 1),
165 which usually mediates protein-protein interactions (35), we proceeded to see if TbPH1-V5 has an
166 interaction partner by immunoprecipitation (IP) via its C-terminal epitope tag. To enrich for soluble
167 TbPH1-V5 and augment IP stringency, we followed the previously described fractionation technique

168 above and used fraction SN3 as the input (Fig. 3A). A mock IP control using the parental cell line
169 without an expressed V5 epitope was performed in parallel.

170 After confirming immunocapture of TbPH1-V5 in the first eluate (Fig. 3A), the IP eluate from this and
171 the mock control were resolved on an SDS-PAGE gel. Sypro Ruby staining showed two prominent
172 bands of ~117 kDa (Fig. 3B, B1), the expected size for TbPH1-V5, and of ~80 kDa (Fig. 3B, B2).
173 Importantly, these bands were not observed in the mock control, indicating their presence is not due
174 to unspecific binding to the magnetic beads used to immobilize the anti-V5 antibody. Mass
175 spectrometry analysis of these two bands identified TbPH1 itself as expected and a previously
176 uncharacterised kinetoplastid-specific kinesin (Tb927.9.15470) (S1 Dataset), which we call TbKifX2
177 based on a previously proposed kinesin nomenclature (19). In contrast to TbPH1, TbKifX2's kinesin
178 motor domain contains a conventional Walker A motif. This motor domain is located on the N-
179 terminus, indicating that TbKiFX2 most likely actively moves toward the plus-end of MTs (36). It also
180 contains a CC domain and two serine phosphorylation sites (30), similarly to TbPH1 (Fig. 1).

181 Interaction between these two proteins was further verified by tagging TbKifX2 with a C-terminal HA
182 tag in the TbPH1-V5 cell line. Indeed, TbKifX2 mirrored the fractionation pattern of TbPH1-V5 (Fig.
183 3C). As before, the SN3 fraction was used as an input for TbKifX2-HA IP, which co-
184 immunoprecipitated TbPH1-V5. Thus, we verified that TbPH1 and TbKifX2 exhibit a strong
185 interaction that persists even in 300 mM NaCl.

186 Whole cells expressing TbPH1-V5 and TbKifX2-HA were fixed and permeabilized prior to incubation
187 with antibodies recognizing either epitope-tag (Fig. 3D). We observed that both proteins possess a
188 considerable cell body signal that appears to be nucleus-excluded, with a prominent hook-like signal
189 along the proximal region of the flagellum. This pattern is consistent with the TrypTag localization
190 data, which visualized mNeonGreen-tagged proteins in immobilized live cells (37). The cell body
191 signal likely represents the cytosolic population of both proteins that was also observed in our
192 fractionation data (Figs. 2A and 3C).

193 **Proximity proteomics reveals the spatial organization and interactors of TbPH1 and TbKifX2**

194 Since conventional IP of TbPH1-V5 under high salt conditions identified only TbKifX2 as its major
195 interaction partner, we sought a different method to identify potential cargo and/or interactors of
196 this putative kinesin complex. To do this, we tagged TbPH1 with a C-terminal biotin ligase 'BioID2'
197 (38), appended with an HA tag (39), to facilitate proximity-dependent biotin identification (BioID) of
198 neighbouring proteins. First, we determined by IFA on permeabilized whole cells using anti-HA
199 antibody that TbPH1-BioID2-HA localizes adjacent to the kinetoplast, which was also observed for
200 TbPH1-V5 (Figs. 2B and 4A). TbPH1-BioID2-HA also exhibited biotinylation activity in this part of the
201 cell, as visualized by streptavidin-conjugated to Alexa Fluor 488 (Fig. 4B). Thus, we confirmed that
202 the chimeric protein is properly localized and appears to biotinylate TbPH1 itself or proximal
203 proteins.

204 Purification of biotinylated proteins was performed as described elsewhere (40) (S2 Fig.). Western
205 blotting revealed that the vast majority of TbPH1-BioID2-HA was present in the soluble S1 fraction
206 (Fig. 4C), which was used for subsequent analysis. At first glance, this result appears to disagree with
207 previous findings from the 'MT sieving' fractionation, which employs comparable amounts of non-
208 ionic detergent and buffers of low ionic strength; however, we should emphasise that 'MT sieving'
209 fractionation uses a different detergent for a shorter incubation time and at a lower temperature in
210 comparison to the BioID purification (see Methods), which likely explains this difference.

211 Next, the S1 fraction was incubated with streptavidin-coated magnetic beads to capture biotinylated
212 proteins, which were subsequently trypsinized on beads prior to liquid chromatography-tandem
213 mass spectroscopy (LC-MS/MS). A mock control using the parental cell line lacking BioID2 expression
214 was processed in parallel. A total of 1,131 proteins were detected with high confidence (Andromeda
215 Protein Score ≥20; >1 unique peptide per protein) (S2 dataset). Following imputation of missing
216 values, seven proteins were shown to be preferentially biotinylated by TbPH1-BioID2-HA, as
217 visualised by plotting the -10 log t-test p value versus the t test difference in a volcano plot (Fig. 4D).
218 Statistically significant hits are found above the cut-off curve in this plot.

219 TbKifX2 was the most enriched protein based on both parameters, consistent with its strong
220 interaction with TbPH1. As expected, TbPH1 is also among the enriched proteins, indicating that
221 TbPH1-BioID2-HA biotinylated itself and/or a nearby untagged, endogenous form of the kinesin-like
222 protein. The sub-cellular location of the five novel proteins was determined using the TrypTag
223 protein localization resource (37). This allowed us to already exclude one of them (Tb927.10.12110)
224 as a contaminant, given its nuclear localization. A putative kinesin with a C-terminal PH domain
225 (Tb927.6.2880) is enriched in the basal body. Two proteins are enriched in the flagellar pocket: a
226 dynamin-like protein 1/2 (DLP2, Tb927.3.4760; DLP1, Tb927.3.4720) and a flagellar pocket protein
227 FP45 (Tb927.9.9730). DLP1/2 is involved in clathrin-mediated endocytosis (41, 42) as well as in
228 mitochondrial scission (41, 43)**.** Interestingly, FP45 has also been demonstrated to be a soluble
229 protein that associates with the membrane surrounding the flagellar pocket by immunogold
230 labelling in an independent study (13). Furthermore, TrypTag localization of FP45 often
231 demonstrates a line emanating from the flagellar pocket toward the anterior of the cell, similar to Tb
232 KifX2 and TbPH1. Only a putative flavin-trafficking protein (Tb927.8.1950) does not have a TrypTag
233 localization entry at this time. However, this protein was found among those that interact with
234 TOEFAZ1, a protein that associates with the tip of the extending FAZ (Fig. 4E) (28). Furthermore,
235 Hilton and colleagues N-terminally tagged Tb927.8.1950 to determine its localization by IFA, which
236 exhibited an enriched signal in the vicinity of the kinetoplast.

237 These observations confirm the tight interaction between TbPH1 and TbKifX2. They also suggest that
238 these proteins associate with the basal body, a cytoskeletal element near the flagellar pocket, as
239 well as the FAZ given the localization of the biotinylated proteins. Indeed, both TbPH1 and TbKifX2
240 were also found within the TOEFAZ1-BioID proxisome with high statistical significance (P=0.001138
241 and 0.0032861, respectively), along with DLP1/2 (P=0.029631) (Fig. 4E) (28). Furthermore, among
242 the most enriched proteins that were biotinylated by TbPH1-BioID2-HA, but just below the statistical
243 significance threshold, was a kinesin (Tb927.8.6830) that was found: 1) in the distal part of the FAZ
244 according to the TrypTag project; 2) within the TOEFAZ1 interactome with very high confidence
245 ($P=9.8 \times 10^{-6}$). Thus, we proceeded to test the basal body and FAZ localization suggested by the
246 TbPH1-BioID (Fig. 4) and IFA (Fig. 2A, 3D) results.

247 **TbPH1 and TbKifX2 localize to the microtubule quartet within the cytoskeleton**

248 We next decided to address whether TbPH1 and TbKifX2 localize to or near the FAZ, as was
249 suggested by the TbPH1 proxisome. Cytoskeletons were detergent-extracted from the TbPH1-V5 and
250 TbKifX2-HA expressing cells to visualize any potential localization to discrete cytoskeletal structures.
251 Indeed both proteins co-localized to a long structure running along the long-axis of the cytoskeleton
252 adjacent to the flagellum (Fig. 5A). Furthermore, detergent extraction solubilized the cell body signal
253 (Fig. 3D), confirming it represented the cytosolic population of TbPH1 and TbKifX2 (Figs 2A and 3C).

254 We proceeded to identify specifically which cytoskeletal element TbPH1 and TbKifX2 associate with.
255 We used antibody recognizing TbKifX2-HA as a proxy for the TbKifX2-TbPH1 complex because of

256 their demonstrated tight interaction (Fig 3), and their co-localization on detergent-extracted
257 cytoskeletons (Fig. 5A). We found TbKifX2-HA to be juxtaposed with the FAZ filament, although the
258 former extended further toward the proximal region of the flagellum (Fig. 5B). This was confirmed
259 by TbKifX2-HA's co-localization with the basal bodies (Fig. 5C). This pattern led us to investigate
260 whether the kinesin was bound to the MtQ, as it originates close to the basal body and is considered
261 a part of the FAZ (7, 8). Indeed, TbKifX2 shows co-localization with a monoclonal antibody 1B41
262 recognizing the MtQ (44) (Fig. 5D).

263 To verify that TbKifX2 indeed binds the MtQ, we employed expansion microscopy (ExM) that
264 enlarges cells by embedding them within a swellable polyacrylamide matrix prior to immunolabelling
265 to allow examination of cellular structures in greater detail (45), and has recently been implemented
266 in *T. brucei* (46, 47). Performing ExM on the TbPH1-V5 and TbKifX2-HA-expressing cell line we
267 observed a punctate signal of an anti-V5 or anti-HA antibody in the cell body (Fig. 5E), consistent
268 with the significant cytosolic fraction of both proteins (Figs. 2A, 3C-D). Moreover, in some cells
269 localization of TbPH1-V5 or TbKifX2-HA to the part of the MtQ, which spirals around the flagellar
270 pocket, was apparent (Fig. 5F); this part of the MtQ is prominent in these ExM preparations (47). The
271 associated V5 or HA signal was not discernible beyond the point of the MtQ joining the corset MTs,
272 where the signal of FAZ constituents, such as ClpGM6 (48), starts (S3 Fig.).The fact, that the signal of
273 TbPH1-V5 or TbKifX2-HA was apparent only in the part of the MtQ around the flagellar pocket is
274 consistent with this being the region of the highest concentration of the proteins in the cell based on
275 IFA, as well as with a lower sensitivity of ExM due to dilution of epitopes stemming from specimen
276 expansion. Taken altogether, ExM reveals that TbPH1 and TbKifX2 bind to the MtQ element of the *T.*
277 *brucei* cytoskeleton.

278 **Depletion of TbPH1 and TbKifX2 causes prominent morphological defects to the posterior end of *T.***
279 ***brucei***

280 To assay the function of the novel kinesin TbKifX2 and its associated kinesin-like protein TbPH1, we
281 depleted their expression by doxycycline-induced RNAi in the cell line expressing TbPH1-V5 and
282 TbKifX2-HA. The downregulation of either protein alone only marginally affected the growth of *T.*
283 *brucei* in comparison to the non-induced cells, despite efficient depletion of each of the respective
284 tagged proteins (Fig. 6A, S4A Fig.). After 6 days of RNAi-silencing of TbKifX2, we fractionated the
285 cytoskeleton from the cytosol under low salt conditions (Fig. 6B). Consistent with 'MT sieving'
286 fractionation (Figs. 2A and 3C) and IFA (Figs 5A and 5B), western blot detection revealed TbKifX2-HA
287 and TbPH1-V5 in both cytoskeletal and cytosolic fractions in cells grown in the absence of
288 tetracycline, in which neither protein was downregulated (Fig. 6B). However, TbPH1 was
289 preferentially depleted from the cytoskeleton fraction upon TbKifX2 silencing. This result indicates
290 that TbKifX2 recruits TbPH1-V5 to the MtQ (Fig. 6B).

291 To get a more robust RNAi phenotype for phenotypic analysis, we generated cell lines in which both
292 proteins were downregulated, which showed more pronounced growth inhibition than the single
293 knock-downs (Fig. 6A). Growth slowed after 3 days of RNAi induction and did not reach levels of the
294 uninduced counterparts at any point during the 7 day time course (S4B Fig.). Depletion of both
295 proteins was confirmed by western blotting (S4B Fig., inset), although neither protein was decreased
296 below the detection limits of this assay.

297 Because both TbPH1 and TbKifX2 are modified in a way suggestive of post-translational regulation
298 (Fig. 1), plus both associate with proteins that may regulate the cell cycle (*e.g.* FP45) (13) and do play
299 a role in cytokinesis (*e.g.* TOEFAZ1/Cif1) (49, 50)**,** we wondered whether the growth inhibition of the
300 double RNAi knockdown is due to a cell cycle defect. Thus, we assayed the proportion of cell cycle

301 stages present over a course of 7 days of TbPH1/TbKifX2 depletion, sorting individual DAPI-stained
302 cells into different cell cycle stages by scoring their number of nuclei (N) and kinetoplasts (K) (3). The
303 proportion of 1N1K cells decreased while 2N2K cells doubled at the same time from around 10% of
304 the population to about 20% (S4C Fig.). The number of zoids (cells with 1 kinetoplast and lacking a
305 nucleus) reached a peak at day 5, making up about 7% of the population, which may suggest
306 problems with cytokinesis. However, we did not observe the consequent emergence of 2N1K or
307 multinucleated cells, arguing against a specific cytokinesis defect (3). Thus, we conclude that TbKifX2
308 and TbPH1 likely do not play a direct role in cell cycle progression and cytokinesis, and thus looked
309 for other phenotypes that would explain the decreased fitness of these cells.

310 We assayed the MtQ and FAZ by IFA after 5 days of RNAi depletion and observed no defects in either
311 of these structures, indicating that TbPH1 and TbKifX2 do not play a role in their biogenesis (S4D
312 Fig.). The lack of an effect on these structures is also consistent with the notion that these proteins
313 do not have a role in cytokinesis. However, by phase contrast microscopy we noticed the emergence
314 of two morphological phenotypes, namely multiple cells joined together on their posterior end, a
315 phenotype resembling abscission defects (51, 52) and single cells with protrusions from the posterior
316 end (Fig. 6D).

317 To better visualize these phenotypes, we observed these cells by scanning electron microscopy (Fig.
318 6D). While control cells showed normal trypomastigote morphology (Fig. 6D), we regularly observed
319 cells with multiple protrusions (arrows) originating from the posterior end in the induced population
320 (Fig. 6D). The occurrence of these cell types was also corroboratively found in transmission electron
321 microscopy, which in addition provided evidence that these protrusions appear to contain normal
322 cellular contents and were surrounded by subpellicular MTs (S5A Fig.). Moreover, the flagellar
323 pocket region appeared to be unaffected by depletion of TbPH1/TbKifX2 (S5B and C Fig.).

324 This effect of TbPH1/TbKifX2-depletion resembled the RNAi-phenotype of two tubulin-tyrosine-
325 ligase-like (TTLL) proteins, which post-translationally modify the C-terminal tails of α- and β-tubulin
326 by addition of polyglutamate side chains (53). Upon depletion of either TTLL, protrusions were
327 observed emanating from the posterior end, which prompted the authors to name this
328 morphological change the 'glove' phenotype. To determine whether TbPH1/TbKifX2 downregulation
329 truly phenocopies that of each TTLL, we immunodecorated cells 5 days post RNAi-induction with
330 antibodies recognizing glutamyl side chains (GT335 antibody) and tyrosinated α-tubulin (YL 1/2
331 antibody); the latter antibody was used previously to visualize the basal bodies (Fig. 5C). Upon
332 depletion of either TTLL, polyglutamylation was decreased and α-tubulin tyrosination increased in
333 the posterior end, from which the protrusions emerged (53). We did not observe either of these
334 changes in post-translational modifications upon TbPH1/TbKifX2 silencing by observing them on
335 individual cells by IFA (S5D Fig.) or the whole cell population by western blot analysis (S5E Fig.),
336 suggesting the mechanism underlying the emergence of posterior-end protrusions differs from that
337 of the TTLLs.

338

339 **DISCUSSION**

340 Kinesins and related kinesin-like proteins constitute one of the largest protein families encoded by
341 the *T. brucei* genome (16) and are represented by diverse gene repertoires in other trypanosomatids
342 as well (17–20). Among the eukaryotes, trypanosomatids have experienced one of the largest
343 expansions of the kinesin motor superfamily, suggesting these proteins endow trypanosomes with
344 unique biological properties, many of which still await elucidation (16, 19, 20). Indeed, this

345 expansion has resulted in the emergence of two trypanosomatid-specific clades of kinesins, named
346 X-1 and X-2. A kinesin belonging to the former, named FCP2/TbKinX1, has been shown to maintain a
347 connection of a new flagellum's distal tip along the side of the old flagellum, thus facilitating the
348 unique mechanism of templated replication of this cytoskeletal organelle in *T. brucei* (29).

349 In this work, we have shed light on the function of a member of the trypanosomatid-specific X-2
350 clade, which we named TbKifX2. We show that TbKifX2 is localized to the MtQ component of the
351 cytoskeleton while maintaining a cytosolic fraction. Previously, TbSpef1 (13) and three other
352 proteins of the TbSpef1 proxisome (14) were found to be localized to the MtQ of kinetoplastids.
353 However, these proteins are located exclusively on the proximal end of the MtQ, in the region
354 between the basal body and the flagellar collar. While TbKifX2 is enriched in this part of the MtQ,
355 this is to our knowledge the first protein identified to be also distributed along the entire length of
356 the MtQ.

357 TbKifX2 recruits TbPH1, a kinesin-like protein with a C-terminal PH domain, to the MtQ. The
358 proposed complex formation is based on our observation that TbPH1 mainly interacts with TbKifX2
359 with a strong affinity that defies high salt concentrations, a condition that usually subverts non-
360 covalent interactions between the CC domains (54). It is rather uncommon for a kinesin to interact
361 with a protein with a kinesin-like structure, but still being catalytically inactive, with the most
362 extensively characterized example being the budding yeast Kar3 kinesin and Vik1, which confers to
363 the Kar3/Vik1 complex a strong interaction with a microtubule (55). We hypothesize that the
364 TbKifX2/TbPH1 complex may represent an adaptation for binding the MtQ. How the TbKifX2/TbPH1
365 complex preferentially interacts with the MtQ over the corset microtubules is an intriguing question.
366 It has been suggested that the MtQ contains β-tubulin with a unique but still unknown modification
367 that is recognized by the 1B41 monoclonal antibody (44, 56), and could have an increased affinity to
368 the kinesin complex investigated here. Alternatively, the kinesins could be activated at a specific site,
369 for example at the proximal end of the MtQ, similar to the yeast kinesin Kip2 being recruited to the
370 minus ends of microtubules by the activity of the spindle pole bodies (57). Whether this is indeed
371 the case, and how such a complex would move along the MtQ (55), remain interesting questions for
372 future research.

373 The TbPH1 proxisome obtained *via* BioID labelling revealed interesting properties of TbPH1 and
374 TbKifX2. First, most of the proteins identified in our study were also observed in the TOEFAZ1/CIF1
375 proxisome with high confidence (28). This verifies our localization of TbKifX2/TbPH1 along the whole
376 length of the MtQ and not just the proximal end, since TOEFAZ1/CIF1 is enriched in the distal tip of a
377 newly formed FAZ, which also incorporates a new MtQ (8, 58). Second, the TbPH1 proxisome
378 contains DLP1/2, which are involved in clathrin-mediated endocytosis (41–43) and FP45, which
379 surrounds the flagellar pocket where endocytosis takes place. This result suggests that TbPH1 may
380 transport vesicular cargo, as PH domains have been shown to bind phosphoinositides, ubiquitous
381 phospholipids that pepper cellular membranes (59). Interestingly, another kinesin with a C-terminal
382 PH domain was also found in the TbPH1 proxisome. Third and finally, a putative flavin-trafficking
383 protein was also found to associate with TbPH1 and TOEFAZ1/CIF1 (28). This annotation is based on
384 the presence of an ApbE-like domain, which is common in prokaryotes but a rare occurrence in
385 eukaryotic proteins (60). What an enzyme potentially influencing redox is doing in association with
386 the MtQ is another open question that has been uncovered in this study.

387 Simultaneous depletion of TbPH1 and TbKifX2 does not affect the overall morphology of MtQ or FAZ,
388 indicating these proteins are likely not involved in the biogenesis of these cellular structures. As
389 these single copy organelles must be faithfully replicated during cell proliferation, it is not surprising
390 that the impact of the double knockdown had a minimal impact on the cell cycle. Nevertheless,

391 TbKifX2/ TbPH1 downregulation has a striking morphogenesis phenotype, namely the accumulation
392 of protrusions from the posterior end of *T. brucei*. The intracellular contents of these protrusions
393 appear to be comparable to the rest of the cell and they are also surrounded by subpellicular MTs.
394 Interestingly, these protrusions are reminiscent of the 'glove phenotype' observed upon depletion of
395 two TTLL enzymes, which are responsible for post-translational modifications appending the C-
396 terminal tails of α- and β-tubulin (53).

397 However, at this juncture, we can only speculate about the nature of these posterior extrusions. For
398 one, simultaneous TbPH1 and TbKifX2 depletion did not affect polyglutamylation or tyrosination of
399 tubulins, indicating that these proteins do not play a role in regulating either of these post-
400 translational modifications as is the case for either TTLL (53). Malfunction of regulated
401 polyglutamylation and tyrosination led to mislocalization of EB1, a MT-plus-end-binding protein that
402 binds to the MT corset at the posterior tip (53, 61). It was proposed that EB1 proteins may dock onto
403 tubulins with the aforementioned post-translational modifications (53). So, the malformations seen
404 in TbPH1/TbKifX2 may affect EB1 or other such MT-plus-end-binding proteins, leading to
405 uncontrolled MT growth or aberrant MT organization. However, it should be noted that EB1 was not
406 identified in the TbPH1 proxisome, so any effect on this protein may be an indirect consequence of
407 RNAi-silencing. The protrusions may also be a consequence of delayed or uncoordinated cytokinesis
408 or represent mechanical damage to the posterior ends due to faulty separation of daughter cells at
409 the final stage of cytokinesis. However, arguing against protrusions arising from a putative
410 cytokinesis defect is that they were not observed in *T. brucei* unable to pull apart due to motility
411 defects (52).

412 In summary, we propose the following hypothesis: the TbPH1-TbKifX2 complex moves along the
413 MtQ transporting cargo representing an auxiliary factor for inducing and/or executing morphological
414 changes during cytokinesis at the distal end of FAZ/MtQ. It is likely that TbKifX2 is a plus-end
415 directed motor based on the N-terminal position of the kinesin motor domain in the molecule (36).
416 When TbPH1-TbKifX2 are depleted, this cargo does not reach the anterior end and potentially
417 accumulates at the posterior of the cell instead, thereby causing aberrant organization of MTs,
418 resulting in the observed protrusions. In conclusion, we have discovered a novel kinesin
419 heterocomplex that localizes along the MtQ, which will facilitate understanding of this fascinating
420 structure and how it may impact the gross morphology of trypanosomatids.

421

422 **MATERIALS AND METHODS**

423 **Cells**

424 Procyclic SmOxP9 cells (62) were grown in SDM79 with 1 µg/ml of puromycin. Cell lines bearing
425 epitope tags were grown with 50 µg /ml hygromycin (TbPH1-V5), 15 µg /ml G418 (TbKifX2-HA) and
426 10 µg /ml blasticidin (TbPH1-BioID2-HA). Selection for the RNAi constructs was with 2.5 µg /ml
427 phleomycin (TbKifX2 RNAi, TbPH1 RNAi and TbKifX2+TbPH1 RNAi).

428 **Plasmids and generation of cell lines**

429 For epitope tagging at the endogenous locus with HA and V5, long PCR products were generated
430 with primers TbPH1V5 FW (TTTCTTCCGGTCTTGACTTATTCCGCTCAGGGAAGCTTTATGATTTCTTATGCGA
431 AAAGAGAGTCATACCGCTCCCGTACggttctggtagtggttcc) and TbPH1V5 RV (ATAATAAAGAGGAAGGGAAG
432 GTAAAGTTCAGAAACAAATTCTGTTGGCTCCTGATAACACTCTCATATTTCCTTCACCGCccaatttgagagacctgtg
433 c) and primer TbKifX2HA FW (AACTACAGTTGCAAATGTGCATGATAGGAAGAAGTTGCCTCACGATGGAGC
434 GTTGGAAAGCGGAACATGTCGGAACCGCAggttctggtagtggttcc) and TbKifX2HA RV (CATTTTAAACAATTTC

435 TCCT TCCCTCTTTTTTCACTCATTCATTCATTCATTCATTCACCACCTTCTTTTTTTTTTGCCTcctgtgc) using
436 pPOT-V5-HygR and pPOT-HA-NeoR vectors as templates (based on (63) and modified from pPOTv4
437 (33)). For tagging with the BioID2 ligase (38), a modified version of pPOTv7-Blast-mNG (39) was used
438 with the aforementioned primers for TbPH1 endogenous locus tagging. 50 µl PCR reactions were
439 directly transfected into procyclic SmOxP9 cells using the Amaxa Nucleofactor electroporator and
440 selection occurred approximately 16 hours after electroporation.

441 To create a vector to simultaneously downregulate both TbPH1 and TbKifX2, a fragment of each (as
442 suggested by RNAit2 software (https://dag.compbio.dundee.ac.uk/RNAit/) (64)) was PCR amplified
443 using primers TbPH1-RNAi-Fw (TAATtctagaGTTGCGTGATGAGCTTCAAA), TbPH1-RNAi-Rv
444 (TATAaagcttCTCCTCTAGCACCGTTTTGC), TbKifX2-RNAi-Fw (TAATggatccCACCGCCATTCTGCA AACAA)
445 and TbKifX2-RNAi-Rv (TATAtctagaGTCATTTGCGTGGGCGATAC) and cloned into BamHI-HindIII sites of
446 p2T7-177 (65) in a three way ligation using XbaI as the restriction site in between the two RNAi
447 fragments. The plasmid was linearised with NotI before electroporation.

448 **RNAi and growth curves**

449 Procyclic form cell lines for depletion of either TbPH1 or TbKifX2 were induced at a density of $2x10^6$
450 cells/ml with 1 µg/ml doxycycline and growth monitored daily with a Z2 Coulter Counter Analyzer
451 (Beckman Coulter). Cells were diluted back to the initial cell density every day. Cell lines carrying the
452 vector for simultaneous depletion of TbPH1 and TbKifX2 were induced at a density of $5x10^5$ cells/ml
453 with 1 µg/ml doxycycline and growth monitored daily with a Neubauer counting chamber. Cells were
454 diluted back to the initial cell density every two days.

455 **DAPI counts**

456 For cell cycle analysis, cells either induced or not for depletion of TbKifX2 and TbPH1 were spread on
457 glass slides, the cell suspension allowed to air-dry and the slides then fixed in methanol at -20 °C.
458 Slides were rehydrated for 5 minutes in PBS before a drop of ProLong™ Gold antifade reagent with
459 DAPI (ThermoScientific) was added, a coverslip applied and the slide sealed. At least 200 cells were
460 scored according to the number of nuclei and kinetoplasts per slide.

461 **Cell fractionation via 'microtubule sieving'**

462 To entrap non-soluble and cytoskeletal proteins within the MT corset, a MT sieving technique as
463 described in (32) was employed. The experiment was conducted exactly as described before in (32)
464 (see also S1 Fig.).

465 **V5 immunoprecipitation**

466 For immunoprecipitation (IP) of TbPH1-V5 from procyclic trypanosome lysates, the V5 antibody
467 (Thermo Fisher) was coupled and cross-linked to protein G coated dynabeads (Thermo Scientific)
468 using 6 mg/ml dimethyl pimelidate dihydrochloride in 0.2M triethanolamine. Beads were then
469 washed in IP wash buffer (20 mM Tris-HCl, pH 7.7, 100 mM KCl, 3 mM $MgCl_2$, 0.5% TritonX-100,
470 cOmplete™ EDTA-free protease inhibitor (Roche)) and stored at 4 °C before further usage. For
471 proteomic analysis of TbPH1 interactions, $1x10^9$ PCF cells were pre-fractionated using the MT sieving
472 technique described above. The SN3 lysate was incubated with V5-coupled dynabeads for 24 hours
473 at 4 °C. Following several washes in IP wash buffer, proteins were eluted using low pH glycine buffer.
474 Aliquots were taken of the different steps for western blot analysis.

475

476

477 **Western blots**

478 Cell lysates were prepared by boiling in 1x SDS sample buffer and the equivalent of $2x10^6$ cells (RNAi
479 lines) or $1x10^7$ cells (IP samples) was loaded per well. Following western blotting, PVDF membranes
480 were blocked for 1 hour in 5% milk-PBS. Incubation with primary antibodies (anti-V5 at 1:1,000;
481 ThermoScientific, anti-HA at 1:1,000; ThermoScientific, anti-tubulin at 1:5,000; Sigma) was
482 performed at 4 °C overnight. Secondary antibodies (HRP-coupled anti-mouse or –rabbit IgG; Sigma)
483 were used at a concentration of 1:2,000 and signals were visualised using Clarity Western ECL
484 substrate (Bio-Rad) on a ChemiDoc MP (Bio-Rad).

485 **SYPRO Ruby staining**

486 Following electrophoresis, polyacrylamide gels were placed into fixing solution (7% glacial acetic
487 acid, 50% methanol) for 30 minutes at room temperature. Following another, identical fixation step,
488 the gel was incubated with SYPRO Ruby solution overnight at room temperature. A washing step in
489 washing solution (7% glacial acetic acid, 10% methanol) for 30 minutes at room temperature was
490 followed by three 5 minute washes in milliQ water before imaging on a ChemiDoc MP (Bio-Rad).

491 **Immunofluorescence and cytoskeleton extraction**

492 Approximately $2x10^6$ cells were used per slide. Cells were washed in PBS and fixed in 2.3% PFA in PBS
493 for approximately 30 minutes before being transferred to microscopy slides (ThermoScientific).
494 Following neutralisation in 0.1M glycine in PBS, slides were incubated in methanol at -20° C
495 overnight for permeabilisation. Slides were then rehydrated in PBS and blocked in 1% BSA in PBS for
496 1 hour followed by incubation with primary antibody for 1 hour in a humid chamber. The slides were
497 then washed three times with PBS before incubation in AlexaFluor-conjugated secondary antibody
498 (goat anti-rabbit/mouse, used at 1:1,000; Invitrogen). Following three further washes in PBS, a drop
499 of ProLong Gold Antifade reagent with DAPI (ThermoScientific) was added, a coverslip applied and
500 the slide sealed with nail polish. Slides were imaged with a Zeiss Axioscope or an Olympus FluoView
501 Fv1000 confocal microscope.

502 For immunofluorescence analysis of cells extracted using the 'MT sieving' fractionation method
503 described above the pellet fraction P2 was fixed in 2.3% PFA as described. All subsequent steps were
504 the same as for whole cell immunofluorescence.

505 To extract cytoskeletons conventionally, approximately $1x\ 10^7$ PCF cells were collected and
506 centrifuged at room temperature for 5 min at 800 x g and the supernatant discarded. Thereafter, the
507 cell pellet was washed once in PBS and after resuspension in PBS applied in a drop-wise fashion to
508 Superfrost plus® slides (ThermoScientific). The cells were left to settle before the addition of PEME
509 buffer (100 mM Pipes, pH 6.9, 1 mM $MgSO_4$, 2 mM EGTA, 0.1 mM EDTA) containing 0.5% (v/v) NP-40
510 (Igepal) for 10 seconds. This cytoskeleton extraction was followed by a 10 minute fixation step in 4%
511 PFA. All subsequent steps were as described above for whole cell immunofluorescence.

512 <u>Antibodies used in immunofluorescence</u>

Antibody	Dilution	Origin
anti-HA (produced in rabbit)	1:1,000	Sigma, Catalog #: H6908
anti-V5 (produced in mouse)	1:1,000	ThermoScientific, Catalog #: 377500
1B41 (MtQ)[1]	1:1,000	(44)
L3B2	1:10	(66)
YL1/2	1:50	(67)

GT335	1:2000	Adipogen Life Sciences, Catalog #: AG-20B-0020
[1]IgM purified from hybridoma supernatant and not mouse ascitic fluid as in original report.		

513

514 **Scanning and transmission electron microscopy**

515 For TEM, cell pellets were high-pressure frozen, freeze substituted in the presence of 2% OsO4 in
516 acetone, and embedded into Spi-Pon812 resin (SPI) as described previously (63). For SEM of the
517 TbPH1/TbKifX2 RNAi cell line, cells were fixed in 2.5% glutaraldehyde in 100 mM PBS overnight at
518 4°C and then spotted onto poly-l-lysine-coated glass cover slips. The cells were post-fixed in 2%
519 osmium tetroxide in 100 mM PBS for 1 h at room temperature and finally washed in the same
520 buffer. After dehydration cells were critical-point dried, coated with gold palladium and imaged.

521 **Expansion microscopy**

522 Expansion microscopy samples were prepared as described previously (47). In brief, $1x10^6$ cells were
523 fixed overnight in a solution containing 4% formaldehyde and 4% acrylamide in PBS and adhered to a
524 poly-L-lysine (Sigma, P4707) coated coverslip. The cells were gelated for 30 min at 37°C in PBS
525 supplemented with 19% sodium acrylate, 10% acrylamide, and 0.1% N, N'-Methylenebisacrylamide,
526 0.5% N, N, N´, N´-tetramethylethylenediamine, and 0.5% ammonium persulfate. The specimens
527 were further denatured by a 2 hour incubation at 95°C in a buffer consisting of 50 mM
528 tris(hydroxymethyl)aminomethane-hydrochloride, 200 mM sodium chloride, 200 mM sodium
529 dodecyl sulphate, pH 9.0, and expanded by three 20 min incubations with 15 ml of ultrapure water.

530 Thereafter, the gels were incubated overnight first with a mixture of anti-HA (Cell Signaling
531 Technology, 3724S; used at 1:250) and C3B9 (68, used at 1:10), anti-V5 (Sigma, V8137-.2MG; used at
532 1:250) and C3B9 or anti-ClpGM6 (48, used at 1:200) and C3B9 antibodies, followed by washes and an
533 overnight incubation with a mixture of secondary antibodies (Invitrogen, A11001 and A21428; used
534 at 1:500). Both primary and secondary antibodies were diluted in PBS supplemented with 2% bovine
535 serum albumin. Finally, the gels were washed with ultrapure water.

536 Prior to imaging pieces of gels containing stained expanded cells was transferred to a glass-bottom
537 dish coated with poly-L-lysine, and imaged using a Leica TCS SP8 confocal microscope with an HC PL
538 apochromatic 63x/NA 1.40 oil immersion objective. Z-stacks were acquired with the step size of 100
539 nm. Confocal z-stacks were processed in Fiji (69). 3D reconstructions were performed in the 3D
540 viewer plugin.

541 **BioID**

542 PCF cells (TbPH1-BioID2-HA and SmOxP9 as controls) were grown in the presence of 50 µM biotin for
543 24 hours. For proximity-dependent biotin identification (BioID), 10^9 PCF cells were extracted in PEME
544 buffer (100 mM Pipes, pH 6.9, 1 mM $MgSO_4$, 2 mM EGTA, 0.1 mM EDTA) containing 0.5% (v/v) NP-40
545 (Igepal) for 15 minutes at room temperature resulting in extract E1. Following centrifugation at
546 3,400 x g for 2 minutes, supernatant S1 was created and pellet P1 was further processed by
547 extraction in lysis buffer (0.4% SDS, 500 mM NaCl, 5 mM EDTA, 1 mM DTT, 50 mM Tris-HCl, pH7.4).
548 Another centrifugation step at 16,000 x g for 10 minutes created supernatant S2. Both supernatants,
549 S1 and S2, were then incubated with streptavidin-conjugated Dynabeads (company) for 4 hours at 4
550 °C. An aliquot of flow through samples F1 and F2 were retained for western blotting and the
551 dynabeads were washed five times with PBS. A small sample of the beads was then resuspended in

552 2x SDS PAGE buffer and boiled, while the remainder of the beads was stored at -80 °C until further
553 processing for mass spectrometry analysis.

554 **Mass spectroscopy analysis of captured biotinylated proteins**

555 Trypsin-digestion of captured biotinylated proteins was performed on bead prior to liquid
556 chromatography-tandem mass spectroscopy (LC-MS/MS) as previously described (39). Data was
557 processed using MaxQuant (70) version 1.6.14 which incorporates the Andromeda search engine
558 (71). Proteins were identified by searching a protein sequence database containing *T. brucei brucei*
559 927 annotated proteins (Version 51, TriTrypDB (25), http://www.tritrypdb.org/) supplemented with
560 frequently observed contaminants. Search parameters specified an MS tolerance of 6 ppm, an
561 MS/MS tolerance at 0.5 Da and full trypsin specificity, allowing for up to two missed cleavages.
562 Carbamidomethylation of cysteine was set as a fixed modification and oxidation of methionine and
563 N-terminal protein acetylation were allowed as variable modifications. The experimental design
564 included matching between runs for biological replicates. Peptides were required to be at least 7
565 amino acids in length, with false discovery rates (FDRs) of 0.01 calculated at the levels of peptides,
566 proteins and modification sites based on the number of hits against the reversed sequence
567 database. The obtained data was subsequently processed in Perseus version 1.6.14 as described in
568 (72).

569 **Data availability**

570 The mass spectrometry proteomics data have been deposited to the ProteomeXchange Consortium
571 via the PRIDE partner repository with the dataset identifier PXD025802.

572 **ACKNOWLEDGEMENTS**

573 We thank Keith Gull (University of Oxford), Linda Kohl (Muséum National d'Histoire Naturelle), Bill
574 Wickstead (University of Nottingham), and Ziyin Li (University of Texas Medical School at Houston)
575 for helpful comments, Susanne Kramer (University of Würzburg), Cynthia He (National University of
576 Singapore), and Chris de Graffenried (Brown University) for antibodies, Peter Gorilak (Institute of
577 Molecular Genetics) for assistance with imaging, as well as Karel Harant and Pavel Talacko (BIOCEV,
578 Prague) and Zbyněk Zdráhal and David Potěšil (CEITEC, Brno) for mass spectroscopy analysis on BioID
579 samples and excised bands, respectively. This work was supported by the Czech Science Foundation
580 grants 20-23513S to HH, and 21-09283S and ERC CZ LL1601 to JL, the ERD funds of the Czech
581 Ministry of Education 16_019/0000759 to HH and JL, and BioImaging grant LM2018129 to MV. Work
582 in the VV laboratory was supported by an EMBO Installation Grant and by the J. E. Purkyne
583 Fellowship of the Czech Academy of Sciences.

584 **REFERENCES**

585 1. Wheeler RJ, Scheumann N, Wickstead B, Gull K, Vaughan S. 2013. Cytokinesis in*Trypanosoma*
586 *brucei* differs between bloodstream and tsetse trypomastigote forms: implications for
587 microtubule-based morphogenesis and mutant analysis. Mol Microbiol 90:1339–1355.

588 2. Gull K. 1999. The cytoskeleton of trypanosomatid parasites. Annu Rev Microbiol. Annu Rev
589 Microbiol. pp. 629–655.

590 3. Robinson DR, Sherwin T, Ploubidou A, Byard EH, Gull K. 1995. Microtubule polarity and
591 dynamics in the control of organelle positioning, segregation, and cytokinesis in the
592 trypanosome cell cycle. J Cell Biol 128:1163–1172.

593 4. Sherwin T, Gull K. 1989. Visualization of detyrosination along single microtubules reveals

594 novel mechanisms of assembly during cytoskeletal duplication in trypanosomes. Cell 57:211–
595 221.

596 5. Field MC, Carrington M. 2009. The trypanosome flagellar pocket. Nat Rev Micro 7:775–786.

597 6. Albisetti A, Florimond C, Landrein N, Vidilaseris K, Eggenspieler M, Lesigang J, Dong G,
598 Robinson DR, Bonhivers M. 2017. Interaction between the flagellar pocket collar and the
599 hook complex via a novel microtubule-binding protein in *Trypanosoma brucei*. PLoS Pathog
600 13:e1006710.

601 7. Lacomble S, Vaughan S, Gadelha C, Morphew MK, Shaw MK, McIntosh JR, Gull K. 2009.
602 Three-dimensional cellular architecture of the flagellar pocket and associated cytoskeleton in
603 trypanosomes revealed by electron microscope tomography. J Cell Sci 122:1081–1090.

604 8. Sunter JD, Gull K. 2016. The Flagellum Attachment Zone: 'The Cellular Ruler' of Trypanosome
605 Morphology. Trends Parasitol. Elsevier Ltd. pp. 309–324.

606 9. Sinclair AN, de Graffenried CL. 2019. More than Microtubules: The Structure and Function of
607 the Subpellicular Array in Trypanosomatids. Trends Parasitol. Elsevier Ltd. pp. 760–777.

608 10. Wheeler RJ, Gull K, Sunter JD. 2019. Coordination of the cell cycle in trypanosomes. Annu Rev
609 Microbiol 73:133–154.

610 11. Woodward R, Gull K. 1990. Timing of nuclear and kinetoplast DNA replication and early
611 morphological events in the cell cycle of *Trypanosoma brucei*. J Cell Sci 95 (Pt 1):49–57.

612 12. Lacomble S, Vaughan S, Gadelha C, Morphew MK, Shaw MK, McIntosh JR, Gull K. 2010. Basal
613 body movements orchestrate membrane organelle division and cell morphogenesis in
614 Trypanosoma brucei. J Cell Sci 123:2884–2891.

615 13. Gheiratmand L, Brasseur A, Zhou Q, He CY. 2013. Biochemical characterization of the bi-lobe
616 reveals a continuous structural network linking the bi-lobe to other single-copied organelles
617 in *Trypanosoma brucei*. J Biol Chem 288:3489–3499.

618 14. Dong X, Lim TK, Lin Q, He CY. 2020. Basal Body Protein TbSAF1 Is Required for Microtubule
619 Quartet Anchorage to the Basal Bodies in *Trypanosoma brucei*. mBio 11:e00668-20.

620 15. Hirokawa N, Noda Y. 2008. Intracellular transport and kinesin superfamily proteins, KIFs:
621 Structure, function, and dynamics. Physiol Rev 88:1089–1118.

622 16. Berriman M, Ghedin E, Hertz-Fowler C, Blandin G, Renauld H, Bartholomeu DC, Lennard NJ,
623 Caler E, Hamlin NE, Haas B, Böhme U, Hannick L, Aslett MA, Shallom J, Marcello L, Hou L,
624 Wickstead B, Alsmark UCM, Arrowsmith C, Atkin RJ, Barron AJ, Bringaud F, Brooks K,
625 Carrington M, Cherevach I, Chillingworth TJ, Churcher C, Clark LN, Corton CH, Cronin A, Davies
626 RM, Doggett J, Djikeng A, Feldblyum T, Field MC, Fraser A, Goodhead I, Hance Z, Harper D,
627 Harris BR, Hauser H, Hostetler J, Ivens A, Jagels K, Johnson D, Johnson J, Jones K, Kerhornou
628 AX, Koo H, Larke N, Landfear S, Larkin C, Leech V, Line A, Lord A, MacLeod A, Mooney PJ,
629 Moule S, Martin DMA, Morgan GW, Mungall K, Norbertczak H, Ormond D, Pai G, Peacock CS,
630 Peterson J, Quail MA, Rabbinowitsch E, Rajandream MA, Reitter C, Salzberg SL, Sanders M,
631 Schobel S, Sharp S, Simmonds M, Simpson AJ, Tallon L, Turner CMR, Tait A, Tivey AR, Van
632 Aken S, Walker D, Wanless D, Wang S, White B, White O, Whitehead S, Woodward J,
633 Wortman J, Adams MD, Embley TM, Gull K, Ullu E, Barry JD, Fairlamb AH, Opperdoes F,
634 Barrell BG, Donelson JE, Hall N, Fraser CM, Melville SE, El-Sayed NM. 2005. The genome of
635 the African trypanosome *Trypanosoma brucei*. Science 309:416–422.

636 17. El-Sayed NM, Myler PJ, Bartholomeu DC, Nilsson D, Aggarwal G, Tran AN, Ghedin E, Worthey
637 EA, Delcher AL, Blandin G, Westenberger SJ, Caler E, Cerqueira GC, Branche C, Haas B,

638 Anupama A, Arner E, Åslund L, Attipoe P, Bontempi E, Bringaud F, Burton P, Cadag E,
639 Campbell DA, Carrington M, Crabtree J, Darban H, Da Silveira JF, De Jong P, Edwards K,
640 Englund PT, Fazelina G, Feldblyum T, Ferella M, Frasch AC, Gull K, Horn D, Hou L, Huang Y,
641 Kindlund E, Klingbeil M, Kluge S, Koo H, Lacerda D, Levin MJ, Lorenzi H, Louie T, Machado CR,
642 McCulloch R, McKenna A, Mizuno Y, Mottram JC, Nelson S, Ochaya S, Osoegawa K, Pai G,
643 Parsons M, Pentony M, Pettersson U, Pop M, Ramirez JL, Rinta J, Robertson L, Salzberg SL,
644 Sanchez DO, Seyler A, Sharma R, Shetty J, Simpson AJ, Sisk E, Tammi MT, Tarleton R, Teixeira
645 S, Van Aken S, Vogt C, Ward PN, Wickstead B, Wortman J, White O, Fraser CM, Stuart KD,
646 Andersson B. 2005. The genome sequence of *Trypanosoma cruzi*, etiologic agent of Chagas
647 disease. Science 309:409–415.

648 18. Ivens AC, Peacock CS, Worthey EA, Murphy L, Aggarwal G, Berriman M, Sisk E, Rajandream
649 MA, Adlem E, Aert R, Anupama A, Apostolou Z, Attipoe P, Bason N, Bauser C, Beck A, Beverley
650 SM, Bianchettin G, Borzym K, Bothe G, Bruschi C V., Collins M, Cadag E, Ciarloni L, Clayton C,
651 Coulson RMR, Cronin A, Cruz AK, Davies RM, De Gaudenzi J, Dobson DE, Duesterhoeft A,
652 Fazelina G, Fosker N, Frasch AC, Fraser A, Fuchs M, Gabel C, Goble A, Goffeau A, Harris D,
653 Hertz-Fowler C, Hilbert H, Horn D, Huang Y, Klages S, Knights A, Kube M, Larke N, Litvin L, Lord
654 A, Louie T, Marra M, Masuy D, Matthews K, Michaeli S, Mottram JC, Müller-Auer S, Munden
655 H, Nelson S, Norbertczak H, Oliver K, O'Neil S, Pentony M, Pohl TM, Price C, Purnelle B, Quail
656 MA, Rabbinowitsch E, Reinhardt R, Rieger M, Rinta J, Robben J, Robertson L, Ruiz JC, Rutter S,
657 Saunders D, Schäfer M, Schein J, Schwartz DC, Seeger K, Seyler A, Sharp S, Shin H, Sivam D,
658 Squares R, Squares S, Tosato V, Vogt C, Volckaert G, Wambutt R, Warren T, Wedler H,
659 Woodward J, Zhou S, Zimmermann W, Smith DF, Blackwell JM, Stuart KD, Barrell B, Myler PJ.
660 2005. The genome of the kinetoplastid parasite, *Leishmania major*. Science 309:436–442.

661 19. Wickstead B, Gull K, Richards TA. 2010. Patterns of kinesin evolution reveal a complex
662 ancestral eukaryote with a multifunctional cytoskeleton. BMC Evol Biol
663 10:https://doi.org/10.1186/1471-2148-10-110.

664 20. Wickstead B, Gull K. 2006. A "Holistic" Kinesin Phylogeny Reveals New Kinesin Families and
665 Predicts Protein Functions. Mol Biol Cell 17:1734–1743.

666 21. Li Z, Lee JH, Chu F, Burlingame AL, Günzl A, Wang CC. 2008. Identification of a Novel
667 Chromosomal Passenger Complex and Its Unique Localization during Cytokinesis in
668 *Trypanosoma brucei*. PLoS One 3:e2354.

669 22. Wickstead B, Carrington JT, Gluenz E, Gull K. 2010. The expanded kinesin-13 repertoire of
670 trypanosomes contains only one mitotic kinesin indicating multiple extra-nuclear roles. PLoS
671 One 5:e0015020.

672 23. Hu L, Hu H, Li Z. 2012. A kinetoplastid-specific kinesin is required for cytokinesis and for
673 maintenance of cell morphology in *Trypanosoma brucei*. Mol Microbiol 83:565–578.

674 24. Wei Y, Hu H, Lun Z-R, Li Z. 2013. The Cooperative Roles of Two Kinetoplastid-Specific Kinesins
675 in Cytokinesis and in Maintaining Cell Morphology in Bloodstream Trypanosomes. PLoS One
676 8:e73869.

677 25. Aslett M, Aurrecoechea C, Berriman M, Brestelli J, Brunk BP, Carrington M, Depledge DP,
678 Fischer S, Gajria B, Gao X, Gardner MJ, Gingle A, Grant G, Harb OS, Heiges M, Hertz-Fowler C,
679 Houston R, Innamorato F, Iodice J, Kissinger JC, Kraemer E, Li W, Logan FJ, Miller JA, Mitra S,
680 Myler PJ, Nayak V, Pennington C, Phan I, Pinney DF, Ramasamy G, Rogers MB, Roos DS, Ross
681 C, Sivam D, Smith DF, Srinivasamoorthy G, Stoeckert CJ, Subramanian S, Thibodeau R, Tivey A,
682 Treatman C, Velarde G, Wang H. 2009. TriTrypDB: A functional genomic resource for the
683 Trypanosomatidae. Nucleic Acids Res 38:D457–D462.

684 26. Bertiaux E, Morga B, Blisnick T, Rotureau B, Bastin P. 2018. A Grow-and-Lock Model for the
685 Control of Flagellum Length in Trypanosomes. Curr Biol 28:3802-3814.e3.

686 27. An T, Li Z. 2018. An orphan kinesin controls trypanosome morphology transitions by targeting
687 FLAM3 to the flagellum. PLOS Pathog 14:e1007101.

688 28. Hilton NA, Sladewski TE, Perry JA, Pataki Z, Sinclair-Davis AN, Muniz RS, Tran HL, Wurster JI,
689 Seo J, de Graffenried CL. 2018. Identification of TOEFAZ1-interacting proteins reveals key
690 regulators of *Trypanosoma brucei* cytokinesis. Mol Microbiol 109:306–326.

691 29. Varga V, Moreira-Leite F, Portman N, Gull K. 2017. Protein diversity in discrete structures at
692 the distal tip of the trypanosome flagellum. Proc Natl Acad Sci U S A 114:E6546–E6555.

693 30. Urbaniak MD, Guther MLS, Ferguson M a J. 2012. Comparative SILAC proteomic analysis of
694 *Trypanosoma brucei* bloodstream and procyclic lifecycle stages. PLoS One 7:e36619.

695 31. Lott K, Li J, Fisk JC, Wang H, Aletta JM, Qu J, Read LK. 2013. Global proteomic analysis in
696 trypanosomes reveals unique proteins and conserved cellular processes impacted by arginine
697 methylation. J Proteomics 91:210–225.

698 32. Fritz M, Vanselow J, Sauer N, Lamer S, Goos C, Siegel TN, Subota I, Schlosser A, Carrington M,
699 Kramer S. 2015. Novel insights into RNP granules by employing the trypanosome's
700 microtubule skeleton as a molecular sieve. Nucleic Acids Res 43:8013–8032.

701 33. Dean S, Sunter J, Wheeler RJ, Hodkinson I, Gluenz E, Gull K. 2015. A toolkit enabling efficient,
702 scalable and reproducible gene tagging in trypanosomatids. Open Biol 5:140197.

703 34. Marx A, Hoenger A, Mandelkow E. 2009. Structures of kinesin motor proteins. Cell Motil
704 Cytoskeleton 66:958–966.

705 35. Burkhard P, Stetefeld J, Strelkov S V. 2001. Coiled coils: A highly versatile protein folding
706 motif. Trends Cell Biol. Trends Cell Biol. pp. 82–88.

707 36. Hirokawa N, Noda Y, Tanaka Y, Niwa S. 2009. Kinesin superfamily motor proteins and
708 intracellular transport. Nat Rev Mol Cell Biol. Nature Publishing Group. pp. 682–696

709 37. Dean S, Sunter JD, Wheeler RJ. 2017. TrypTag.org: A Trypanosome Genome-wide Protein
710 Localisation Resource. Trends Parasitol. Elsevier Ltd. pp. 80–82.

711 38. Kim DI, Jensen SC, Noble KA, Kc B, Roux KH, Motamedchaboki K, Roux KJ. 2016. An improved
712 smaller biotin ligase for BioID proximity labeling. Mol Biol Cell 27:1188–1196.

713 39. Pyrih J, Rašková V, Škodová-Sveráková I, Pánek T, Lukeš J. 2020. ZapE/Afg1 interacts with
714 Oxa1 and its depletion causes a multifaceted phenotype. PLoS One 15:e0234918.

715 40. Morriswood B, Havlicek K, Demmel L, Yavuz S, Sealey-Cardona M, Vidilaseris K, Anrather D,
716 Kostan J, Djinović-Carugo K, Roux KJ, Warren G. 2013. Novel bilobe components in
717 *Trypanosoma brucei* identified using proximity-dependent biotinylation. Eukaryot Cell
718 12:356–367.

719 41. Benz C, Stříbrná E, Hashimi H, Lukeš J. 2017. Dynamin-like proteins in Trypanosoma brucei: A
720 division of labour between two paralogs? PLoS One 12:e0177200.

721 42. Morgan GW, Goulding D, Field MC. 2004. The single dynamin-like protein of *Trypanosoma*
722 *brucei* regulates mitochondrial division and is not required for endocytosis. J Biol Chem
723 279:10692–701.

724 43. Chanez A-L, Hehl AB, Engstler M, Schneider A. 2006. Ablation of the single dynamin of *T.*

725 *brucei* blocks mitochondrial fission and endocytosis and leads to a precise cytokinesis arrest. J
726 Cell Sci 119:2968–74.

727 44. Gallo JM, Précigout E, Schrével J. 1988. Subcellular sequestration of an antigenically unique
728 beta-tubulin. Cell Motil Cytoskeleton 9:175–183.

729 45. Gambarotto D, Zwettler FU, Le Guennec M, Schmidt-Cernohorska M, Fortun D, Borgers S,
730 Heine J, Schloetel JG, Reuss M, Unser M, Boyden ES, Sauer M, Hamel V, Guichard P. 2019.
731 Imaging cellular ultrastructures using expansion microscopy (U-ExM). Nat Methods 16:71–74.

732 46. Amodeo S, Kalichava A, Fradera-Sola A, Bertiaux-Lequoy E, Guichard P, Butter F, Ochsenreiter
733 T. 2021. Characterization of the novel mitochondrial genome segregation factor TAP110 in
734 *Trypanosoma brucei*. J Cell Sci 134:jcs.254300.

735 47. Gorilak P, Pružincová M, Vachova H, Olšinová M, Varga V. 2021. Expansion microscopy
736 facilitates quantitative super-resolution studies of cytoskeletal structures in kinetoplastid
737 parasites. Open Biol 11:210131.

738 48. Hayes P, Varga V, Olego-Fernandez S, Sunter J, Ginger ML, Gull K. 2014. Modulation of a
739 cytoskeletal calpain-like protein induces major transitions in trypanosome morphology. J Cell
740 Biol 206:377–384.

741 49. McAllaster MR, Ikeda KN, Lozano-Núñez A, Anrather D, Unterwurzacher V, Gossenreiter T,
742 Perry JA, Crickley R, Mercadante CJ, Vaughan S, De Graffenried CL. 2015. Proteomic
743 identification of novel cytoskeletal proteins associated with TbPLK, an essential regulator of
744 cell morphogenesis in *Trypanosoma brucei*. Mol Biol Cell 26:3013–3029.

745 50. Zhou Q, An T, Pham KTM, Hu H, Li Z. 2018. The CIF1 protein is a master orchestrator of
746 trypanosome cytokinesis that recruits several cytokinesis regulators to the cytokinesis
747 initiation site. J Biol Chem 293:16177–16192.

748 51. Benz C, Clucas C, Mottram JC, Hammarton TC. 2012. Cytokinesis in bloodstream stage
749 *Trypanosoma brucei* requires a family of katanins and spastin. PLoS One 7:e30367.

750 52. Ralston KS, Lerner AG, Diener DR, Hill KL. 2006. Flagellar motility contributes to cytokinesis in
751 *Trypanosoma brucei* and is modulated by an evolutionarily conserved dynein regulatory
752 system. Eukaryot Cell 5:696–711.

753 53. Jentzsch J, Sabri A, Speckner K, Lallinger-Kube G, Weiss M, Ersfeld K. 2020. Microtubule
754 polyglutamylation is important for regulating cytoskeletal architecture and motility in
755 Trypanosoma brucei. J Cell Sci 133 (18): jcs248047

756 54. Grigoryan G, Keating AE. 2008. Structural specificity in coiled-coil interactions. Curr Opin
757 Struct Biol. Curr Opin Struct Biol. pp. 477–483.

758 55. Allingham JS, Sproul LR, Rayment I, Gilbert SP. 2007. Vik1 Modulates Microtubule-Kar3
759 Interactions through a Motor Domain that Lacks an Active Site. Cell 128:1161–1172.

760 56. Gallo JM, Precigout E. 1988. Tubulin expression in trypanosomes. Biol Cell 64:137–143.

761 57. Chen X, Widmer LA, Stangier MM, Steinmetz MO, Stelling J, Barral Y. 2019. Remote control of
762 microtubule plus-end dynamics and function from the minus-end. Elife 8:1–32.

763 58. Campbell PC, de Graffenried CL. 2020. Alternate histories of cytokinesis: lessons from the
764 trypanosomatids. Mol Biol Cell 31:2631–2639.

765 59. Lemmon MA. 2007. Pleckstrin homology (PH) domains and phosphoinositides. Biochem Soc
766 Symp 74:81–93.

767 60. Schenk R, Bachmaier S, Bringaud F, Boshart M. 2021. Efficient flavinylation of glycosomal
768 fumarate reductase by its own ApbE domain in *Trypanosoma brucei*. FEBS J
769 https://doi.org/10.1111/febs.15812.

770 61. Sheriff O, Lim LF, He CY. 2014. Tracking the biogenesis and inheritance of subpellicular
771 microtubule in *Trypanosoma brucei* with inducible YFP- α-tubulin. Biomed Res Int 2014.

772 62. Poon SK, Peacock L, Gibson W, Gull K, Kelly S. 2012. A modular and optimized single marker
773 system for generating *Trypanosoma brucei* cell lines expressing T7 RNA polymerase and the
774 tetracycline repressor. Open Biol 2:110037.

775 63. Kaurov I, Vancová M, Schimanski B, Cadena LR, Heller J, Bílý T, Potěšil D, Eichenberger C,
776 Bruce H, Oeljeklaus S, Warscheid B, Zdráhal Z, Schneider A, Lukeš J, Hashimi H. 2018. The
777 Diverged Trypanosome MICOS Complex as a Hub for Mitochondrial Cristae Shaping and
778 Protein Import. Curr Biol 28:3393-3407.e5.

779 64. Redmond S, Vadivelu J, Field MC. 2003. RNAit: An automated web-based tool for the
780 selection of RNAi targets in *Trypanosoma brucei*. Mol Biochem Parasitol 128:115–118.

781 65. Wickstead B, Ersfeld K, Gull K. 2002. Targeting of a tetracycline-inducible expression system
782 to the transcriptionally silent minichromosomes of *Trypanosoma brucei*. Mol Biochem
783 Parasitol 125:211–6.

784 66. Kohl L, Sherwin T, Gull K. 1999. Assembly of the paraflagellar rod and the flagellum
785 attachment zone complex during the *Trypanosoma brucei* cell cycle. J Eukaryot Microbiol
786 46:105–109.

787 67. Sherwin T, Schneider A, Sasse R, Seebeck T, Gull K. 1987. Distinct localization and cell cycle
788 dependence of COOH terminally tyrosinolated α-tubulin in the microtubules of *Trypanosoma*
789 *brucei brucei*. J Cell Biol 104:439–446.

790 68. Woods A, Sherwin T, Sasse R, MacRae TH, Baines AJ, Gull K. 1989. Definition of individual
791 components within the cytoskeleton of *Trypanosoma brucei* by a library of monoclonal
792 antibodies. J Cell Sci 93 (Pt 3):491—500.

793 69. Schindelin J, Arganda-Carreras I, Frise E, Kaynig V, Longair M, Pietzsch T, Preibisch S, Rueden
794 C, Saalfeld S, Schmid B, Tinevez JY, White DJ, Hartenstein V, Eliceiri K, Tomancak P, Cardona A.
795 2012. Fiji: An open-source platform for biological-image analysis. Nat Methods. Nature
796 Publishing Group. pp. 676–682.

797 70. Cox J, Mann M. 2008. MaxQuant enables high peptide identification rates, individualized
798 p.p.b.-range mass accuracies and proteome-wide protein quantification. Nat Biotechnol
799 26:1367–1372.

800 71. Cox J, Neuhauser N, Michalski A, Scheltema RA, Olsen J V., Mann M. 2011. Andromeda: A
801 peptide search engine integrated into the MaxQuant environment. J Proteome Res 10:1794–
802 1805.

803 72. Zoltner M, del Pino RC, Field MC. 2020. Sorting the Muck from the Brass: Analysis of Protein
804 Complexes and Cell Lysates, p. 645–653. *In* Methods in Molecular Biology. Humana Press Inc.
805 pp. 645–653.

806 73. Kramer S, Queiroz R, Ellis L, Webb H, Hoheisel JD, Clayton C, Carrington M. 2008. Heat shock
807 causes a decrease in polysomes and the appearance of stress granules in trypanosomes
808 independently of eIF2α phosphorylation at Thr169. J Cell Sci 121:3002–3014.

809

810 **FIGURE LEGENDS**

811 **Fig. 1:** Domain architecture of TbPH1 and TbKifX2. Schematic depiction includes phosphorylation and
812 arginine methylation sites. The consensus Walker A motif is shown in comparison with the
813 respective motifs of TbPH1 and TbKifX2. Key residues in ATP hydrolysis shown in red and mutations
814 in purple. CC: coiled coil domain, PH: pleckstrin homology domain, HDL: homeodomain-like fold.

815 **Fig. 2:** TbPH1-V5 fractionates with the cytoskeleton. **(A)** Western blot of-trypanosome cell fractions.
816 Fractionation procedure is summarized in S1 Fig. Antibodies used were anti-V5 and anti-SCD6 (73). T:
817 total lysate, SN: supernatant, P: pellet. **(B)** IFA of fraction P2. Cells were labelled with anti-V5
818 antibody (green) and DAPI. The scale bar corresponds to 5 µm.

819 **Fig. 3:** TbPH1 interacts with TbKifX2, a kinetoplastid-specific kinesin. **(A)** Western blot verifying
820 immunoprecipitation of TbPH1-V5. The blot was probed with anti-V5 and anti-α-tubulin antibodies.
821 The parental cell line SmOxP9 was used as a control. T: total lysate, SN3: supernatant 3, FT: flow
822 through, E: elution. **(B)** SyproRuby-stained gel of elution fractions of TbPH1-V5 IP and mock control
823 (SmOxP9). B1 and B2: bands excised and identified by mass spectrometry. **(C)** Western blot showing
824 interaction of TbPH1-V5 and TbKifX2-HA. TbKifX2-HA was immunoprecipitated in the same way as
825 PH1-V5. T: total lysate, SN: supernatant, P: pellet, FT: flow through, E: elution. **(D)** IFA on whole cells
826 detecting TbPH1-V5 (top) and TbKifX2-HA (bottom). Cells were counterstained with antibody
827 recognizing α-tubulin (top) and acetylated α-tubulin (bottom).

828 **Fig. 4:** The proxisome of TbPH1. **(A)** IFA showing localisation of TbPH1-BioID2-HA. Cells were labelled
829 with anti-HA (red) and DAPI. The scale bar corresponds to 5 µm. **(B)** IFA showing localisation of
830 biotinylated proteins. Cells were labelled with streptavidin-AF488 (green) and DAPI. The scale bar
831 corresponds to 5 µm. **(C)** Western blot (top panel) and stain-free gel (bottom panel) of a
832 representative BioID experiment. The blot was probed with anti-HA to confirm the presence of
833 TbPH1-BioID2-HA in the respective fractions. E: extract, SN: supernatant, F: flow through, B: boiled
834 beads. **(D)** Volcano plot with -10 log t-test p value plotted against the t-test difference between
835 TbPH1-BioID2-HA sample and mock (SmOxP9 cells) from three biological replicates. Statistically
836 significant hits are found above the curve in the top right quadrant and their identity is indicated.
837 Accession numbers are given with additional annotations in parentheses; these are color coded
838 based on their localization determined by TrypTag (37). **(E)** Heat map of SAINTq score (*i.e.* P value) of
839 proteins interacting with TOEFAZ1 (28), positions of proteins also found in the TbPH1 proxisome are
840 indicated. a: Tb927.8.6830 (kinesin), b: Tb927.3.2490 (PH1), c: Tb927.8.1950 (ApbE-like domain), d:
841 Tb927.9.15470 (KifX2), e: Tb927.3.4720/60 (DLP1/2).

842 **Fig. 5:** TbKifX2 localises to the MtQ. **(A)** IFA on extracted cytoskeletons probing co-localisation of
843 TbKifX2-HA with an HA antibody. Cells were counterstained with anti-V5 to detect TbPH1-V5. **(B)** IFA
844 on extracted cytoskeletons probing co-localisation of TbKifX2-HA with the FAZ. Cells were
845 counterstained with L3B2 (recognising the FAZ filament, green). **(C)** IFA on extracted cytoskeletons
846 probing co-localisation of TbKifX2-HA with anti-HA antibody with basal bodies. Cells were
847 counterstained with YL1/2 (recognising mature basal bodies, green) **(D)** IFA on extracted
848 cytoskeletons probing co-localisation of TbKifX2-HA with the MtQ. Cells were counterstained with
849 mAB 1B41 (recognising the MtQ, green) The scale bar for all IFAs corresponds to 5 µm. **(E)**
850 Ultrastructure expansion microscopy of TbPH1 and TbKifX2. Cells were labelled with anti-V5/HA
851 antibody (purple) and anti-tubulin antibody C3B9 (grey) to visualize the MT corset. Punctate
852 cytosolic signals are visible in these preparations. **(F)** Ultrastructure expansion microscopy of TbPH1
853 and TbKifX2 (close-up view of posterior part of the cell). Cells were labelled with anti-V5/HA

854 antibody (purple) and anti-tubulin antibody C3B9 (grey) to visualize the MT corset. Purple arrows are
855 pointing to the MtQ signal.

856 **Fig. 6:** Depletion of TbPH1 and TbKifX2 affects posterior end remodelling. **(A)** Bar chart showing
857 population doubling times for TbPH1, TbKifX2 and TbPH1/TbKifX2 depletion cell lines. -/+: -/+
858 doxycycline to induce RNAi, the average difference in hours from three experiments is shown above
859 the respective bars. **(B)** Western blot of cellular fractionation experiment following TbKifX2 RNAi.
860 The blot was probed with anti-HA (to detect TbKifX2), anti-V5 (to detect TbPH1) and anti-α-tubulin
861 as a loading control. WCL: whole cell lysate. **(C)** Phase contrast images of TbPH1/TbKifX2 RNAi cells. +
862 tet: induced for 5 days. The scale bar corresponds to 5 µm. Arrows indicate morphological defects.
863 **(D)** Scanning electron microscopy of TbPH1/TbKifX2 RNAi cells. + tet: induced for 5 days. Arrows
864 pointing to posterior end protrusions. The scale bar corresponds to 10 µm.

865 **S1 Fig.:** Schematic depiction of microtubule sieving technique. According to (32).

866 **S2 Fig.:** Schematic depiction of proximity-dependent biotinylation (BioID). According to (40). Only
867 steps in black were performed in our study.

868 **S3 Fig.:** Ultrastructure expansion microscopy of a cell labelled with anti-ClpGM6 (to detect the FAZ,
869 purple) and anti-tubulin antibody C3B9 (grey) to visualize the MT corset.

870 **S4 Fig.:** TbPH1/TbKifX2 RNAi. **(A)** Growth curves of TbPH1 and TbKIfX2 RNAi cell lines. Filled circles:
871 TbKifX2 – tet, open circles: TbKIfX2 + tet, filled triangles: TbPH1 – tet, open triangles: TbPH1 + tet.
872 Insets show western blots probed with anti-HA (to detect TbKifX2), anti-V5 (to detect TbPH1) and
873 anti-α-tubulin as a loading control. **(B)** Growth curve of TbPH1/TbKifX2 RNAi cell line. Filled circles:
874 TbPH1/TbKifX2 – tet, open circles: TbPH1/TbKifX2 + tet. Inset depicts western blot showing
875 depletion of TbPH1/TbKifX2. Samples were taken at the same time as the growth curve in B was
876 performed. The blot was probed with anti-HA (to detect TbKifX2), anti-V5 (to detect TbPH1) and
877 anti-α-tubulin as a loading control. **(C)** Bar chart depicting different cell cycle phases during
878 TbPH1/TbKifX2 RNAi time course. DAPI counts were performed in triplicate with at least 200 cells
879 counted per time point. N: nucleus, K: kinetoplast. **(D)** IFA of TbPH1/TbKifX2 RNAi cells. + tet:
880 induced for 5 days. Extracted cytoskeletons were labelled with L3B2 (recognising the FAZ filament,
881 red), mAB 1B41 (recognising the MtQ, green) and DAPI. The scale bar corresponds to 5 µm.

882 **S5 Fig.:** Transmission electron microscopy and IFA of TbPH1/TbKifX2 RNAi cell line. Cells were
883 induced for 5 days. **(A)** Image depicting posterior end protrusions (arrow). The scale bar corresponds
884 to 1 µm. **(B)** Flagellar pocket region of cells not induced for TbPH1/TbKifX2. The scale bar
885 corresponds to 500 nm. **(C)** Flagellar pocket region of cells induced for TbPH1/TbKifX2 RNAi. The
886 scale bar corresponds to 500 nm. **(D)** IFA on cytoskeletons probing effects of TbPH1/TbKifX2
887 depletion post-translational modifications of tubulin. Cells were counterstained with GT335 (red,
888 staining glutamyl side chains) and YL1/2 (green, staining tyrosinated α-tubulin). The scale bar
889 corresponds to 5 µm. **(E)** Western blots taken after 3 to 5 days (d) of growth in presence (+) or
890 absence (-) of doxycycline probed with antibodies recognizing GT335, YL1/2 and α-tubulin, the last
891 as a loading control.

892 **S1 Dataset:** Mass spectrometry analysis of excised bands B1 and B2 from Fig. 3B.

893 **S2 Dataset:** Mass spectrometry data of TbPH1 BioID experiment. Data with and without imputation
894 and filtered for Andromeda scores >20 and presence of >1 peptide, which was used to
895 generate the volcano plot in Fig. 4D.

896

897 **FIGURES**

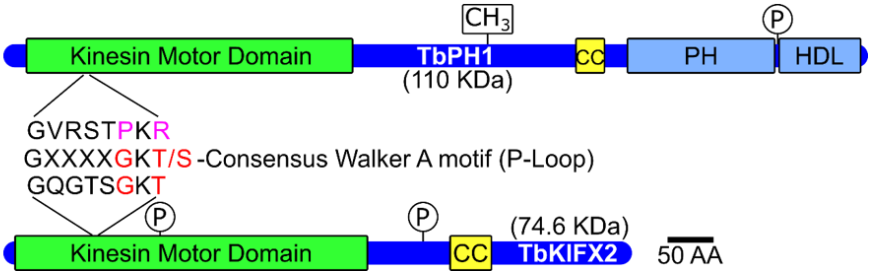

898

899

900 **Fig. 1:** Domain architecture of TbPH1 and TbKifX2. Schematic depiction includes phosphorylation and
901 arginine methylation sites. The consensus Walker A motif is shown in comparison with the
902 respective motifs of TbPH1 and TbKifX2. Key residues in ATP hydrolysis shown in red and mutations
903 in purple. CC: coiled coil domain, PH: pleckstrin homology domain, HDL: homeodomain-like fold.

904

905

906

907

908

909

910

911

912

913

914

915

916

917

918

919

920

921

922

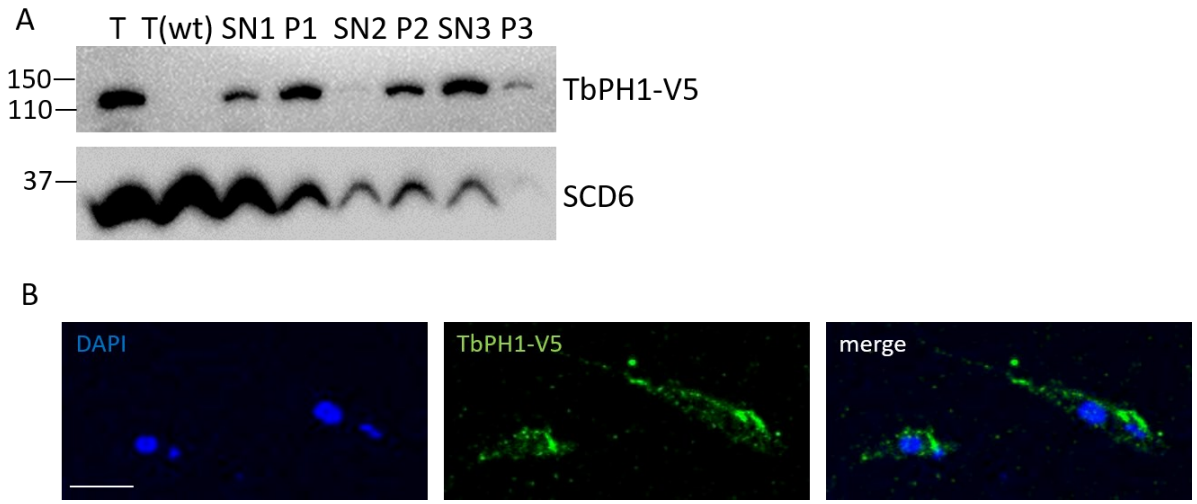

Fig. 2: TbPH1-V5 fractionates with the cytoskeleton. **(A)** Western blot of-trypanosome cell fractions. Fractionation procedure is summarized in S1 Fig. Antibodies used were anti-V5 and anti-SCD6 (73). T: total lysate, SN: supernatant, P: pellet. **(B)** IFA of fraction P2. Cells were labelled with anti-V5 antibody (green) and DAPI. The scale bar corresponds to 5 µm.

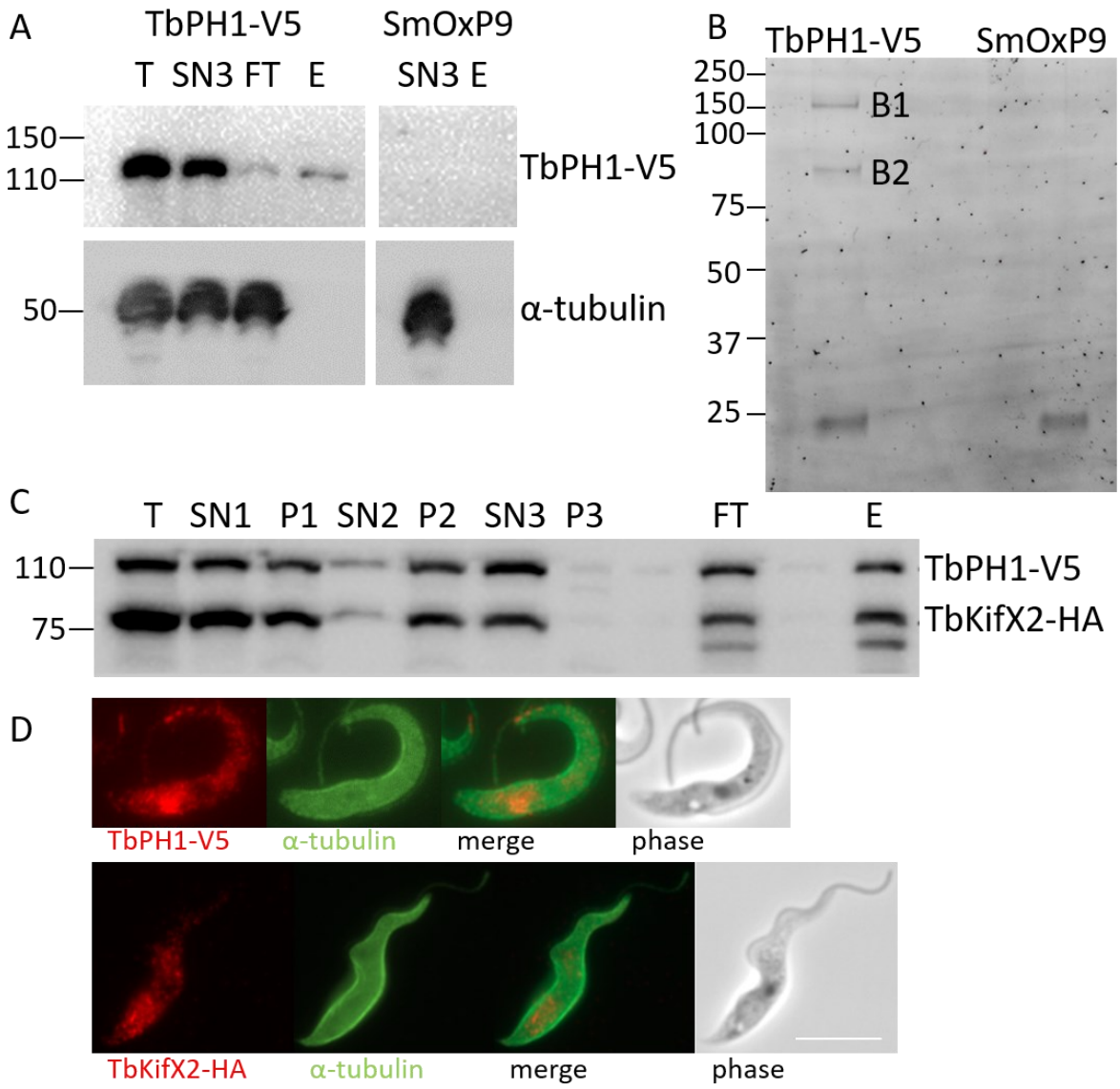

Fig. 3: TbPH1 interacts with TbKifX2, a kinetoplastid-specific kinesin. **(A)** Western blot verifying immunoprecipitation of TbPH1-V5. The blot was probed with anti-V5 and anti-α-tubulin antibodies. The parental cell line SmOxP9 was used as a control. T: total lysate, SN3: supernatant 3, FT: flow through, E: elution. **(B)** SyproRuby-stained gel of elution fractions of TbPH1-V5 IP and mock control (SmOxP9). B1 and B2: bands excised and identified by mass spectrometry. **(C)** Western blot showing interaction of TbPH1-V5 and TbKifX2-HA. TbKifX2-HA was immunoprecipitated in the same way as PH1-V5. T: total lysate, SN: supernatant, P: pellet, FT: flow through, E: elution. **(D)** IFA on whole cells detecting TbPH1-V5 (top) and TbKifX2-HA (bottom). Cells were counterstained with antibody recognizing α-tubulin (top) and acetylated α-tubulin (bottom).

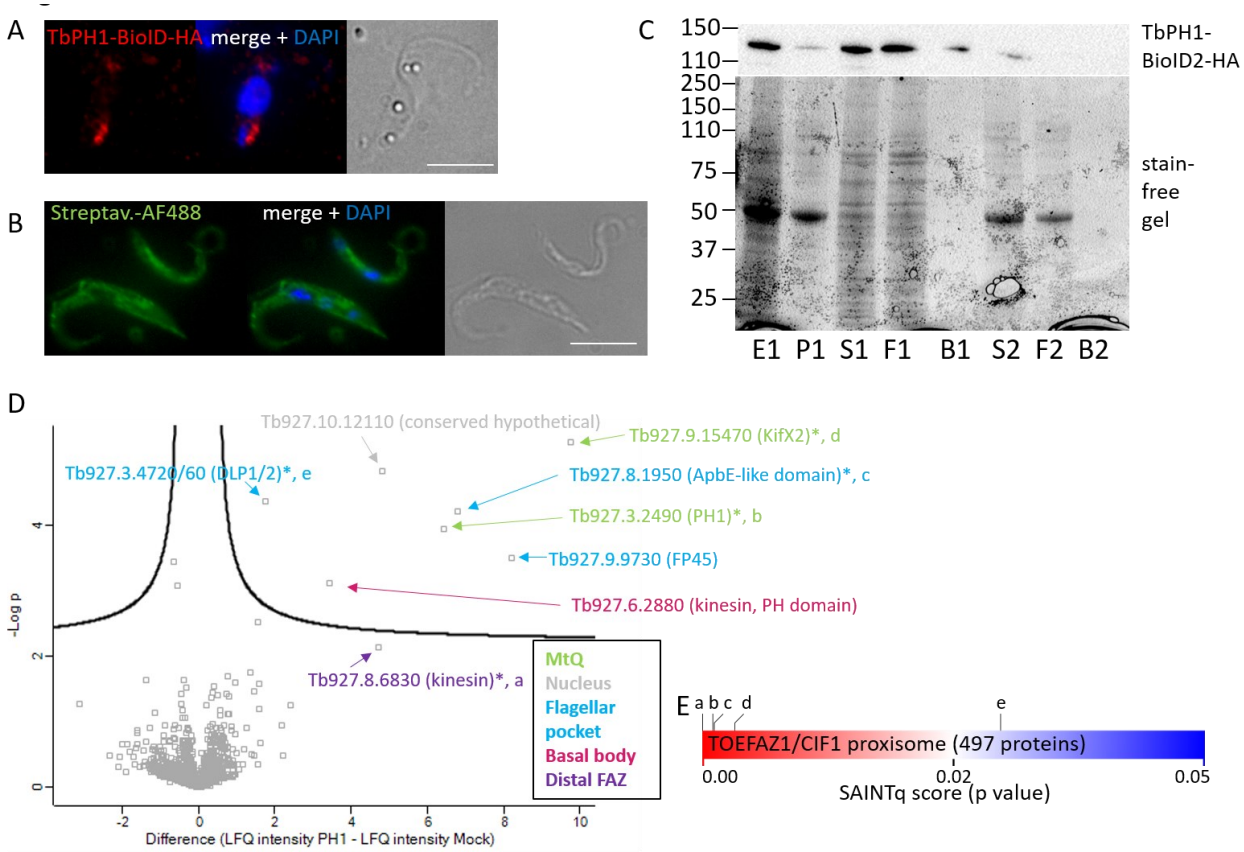

Fig. 4: The proxisome of TbPH1. **(A)** IFA showing localisation of TbPH1-BioID2-HA. Cells were labelled with anti-HA (red) and DAPI. The scale bar corresponds to 5 µm. **(B)** IFA showing localisation of biotinylated proteins. Cells were labelled with streptavidin-AF488 (green) and DAPI. The scale bar corresponds to 5 µm. **(C)** Western blot (top panel) and stain-free gel (bottom panel) of a representative BioID experiment. The blot was probed with anti-HA to confirm the presence of TbPH1-BioID2-HA in the respective fractions. E: extract, SN: supernatant, F: flow through, B: boiled beads. **(D)** Volcano plot with -10 log t-test p value plotted against the t-test difference between TbPH1-BioID2-HA sample and mock (SmOxP9 cells) from three biological replicates. Statistically significant hits are found above the curve in the top right quadrant and their identity is indicated. Accession numbers are given with additional annotations in parentheses; these are color coded based on their localization determined by TrypTag (37). **(E)** Heat map of SAINTq score (*i.e.* P value) of proteins interacting with TOEFAZ1 (28), positions of proteins also found in the TbPH1 proxisome are indicated. a: Tb927.8.6830 (kinesin), b: Tb927.3.2490 (PH1), c: Tb927.8.1950 (ApbE-like domain), d: Tb927.9.15470 (KifX2), e: Tb927.3.4720/60 (DLP1/2).

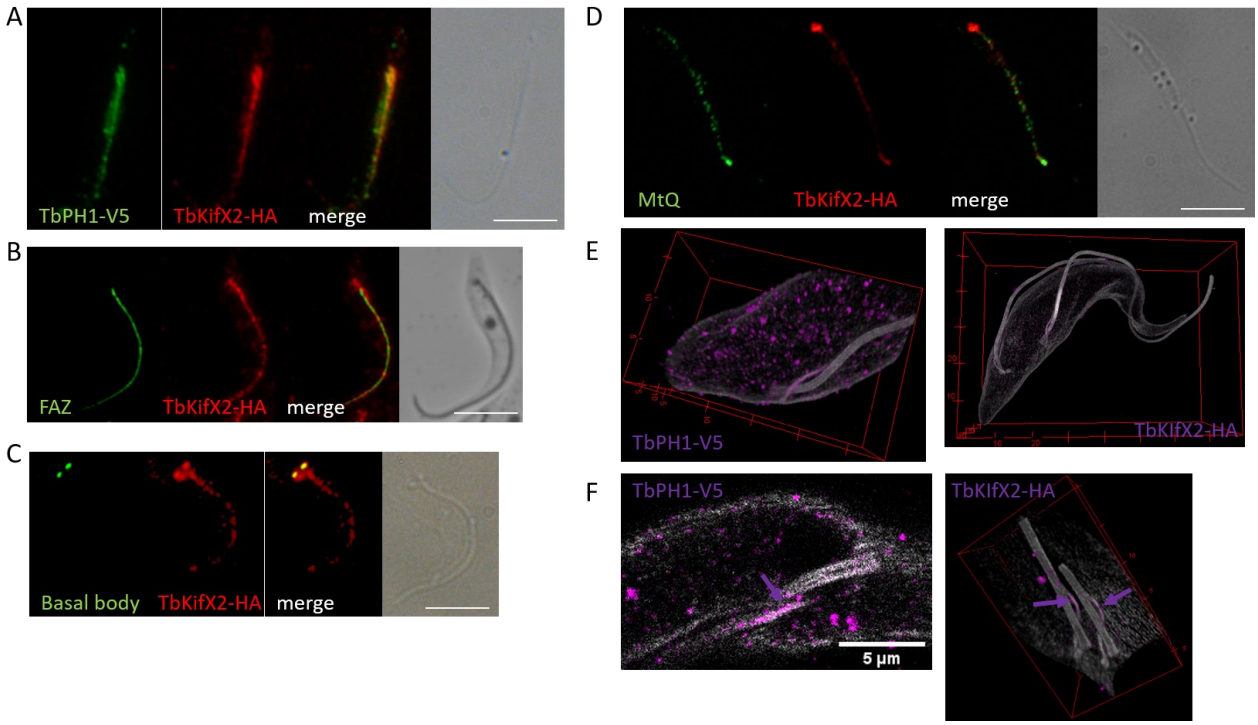

Fig. 5: TbKifX2 localises to the MtQ. **(A)** IFA on extracted cytoskeletons probing co-localisation of TbKifX2-HA with an HA antibody. Cells were counterstained with anti-V5 to detect TbPH1-V5. **(B)** IFA on extracted cytoskeletons probing co-localisation of TbKifX2-HA with the FAZ. Cells were counterstained with L3B2 (recognising the FAZ filament, green). **(C)** IFA on extracted cytoskeletons probing co-localisation of TbKifX2-HA with anti-HA antibody with basal bodies. Cells were counterstained with YL1/2 (recognising mature basal bodies, green) **(D)** IFA on extracted cytoskeletons probing co-localisation of TbKifX2-HA with the MtQ. Cells were counterstained with mAB 1B41 (recognising the MtQ, green) The scale bar for all IFAs corresponds to 5 µm. **(E)** Ultrastructure expansion microscopy of TbPH1 and TbKifX2. Cells were labelled with anti-V5/HA antibody (purple) and anti-tubulin antibody C3B9 (grey) to visualize the MT corset. Punctate cytosolic signals are visible in these preparations. **(F)** Ultrastructure expansion microscopy of TbPH1 and TbKifX2 (close-up view of posterior part of the cell). Cells were labelled with anti-V5/HA

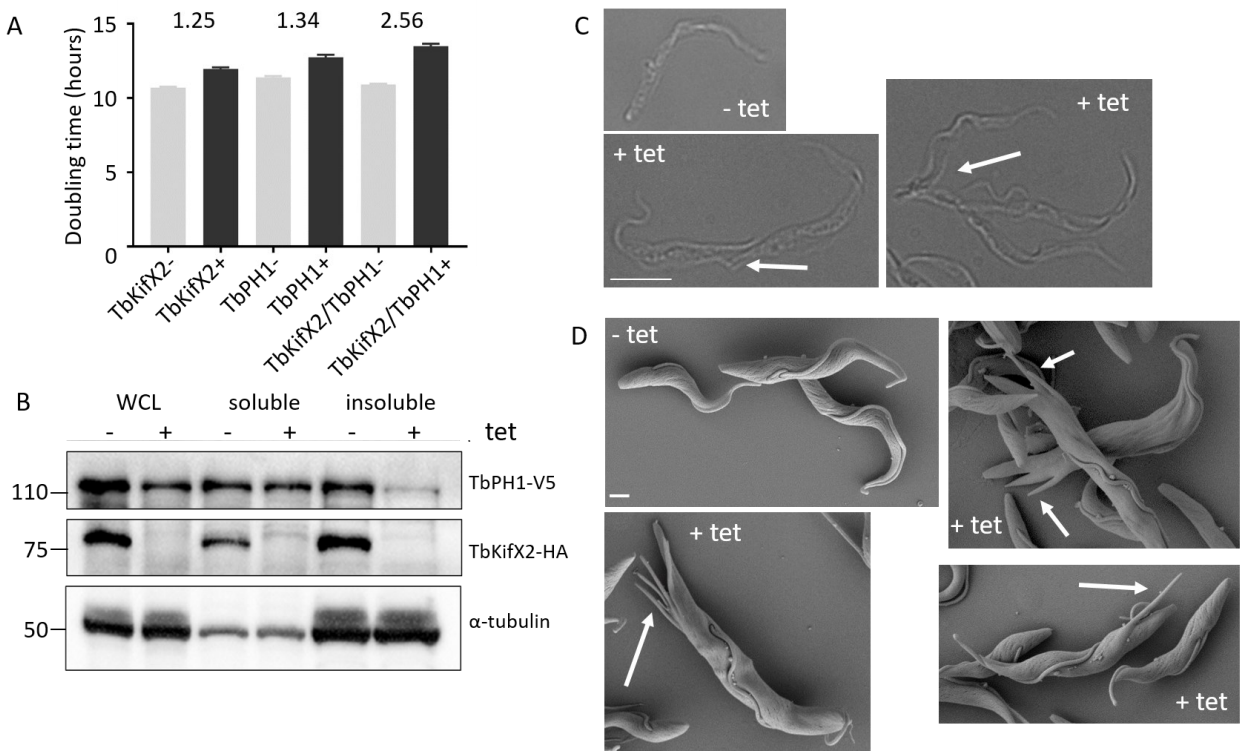

Fig. 6: Depletion of TbPH1 and TbKifX2 affects posterior end remodelling. **(A)** Bar chart showing population doubling times for TbPH1, TbKifX2 and TbPH1/TbKifX2 depletion cell lines. -/+: -/+ doxycycline to induce RNAi, the average difference in hours from three experiments is shown above the respective bars. **(B)** Western blot of cellular fractionation experiment following TbKifX2 RNAi. The blot was probed with anti-HA (to detect TbKifX2), anti-V5 (to detect TbPH1) and anti-α-tubulin as a loading control. WCL: whole cell lysate. **(C)** Phase contrast images of TbPH1/TbKifX2 RNAi cells. + tet: induced for 5 days. The scale bar corresponds to 5 µm. Arrows indicate morphological defects. **(D)** Scanning electron microscopy of TbPH1/TbKifX2 RNAi cells. + tet: induced for 5 days. Arrows pointing to posterior end protrusions. The scale bar corresponds to 10 µm.

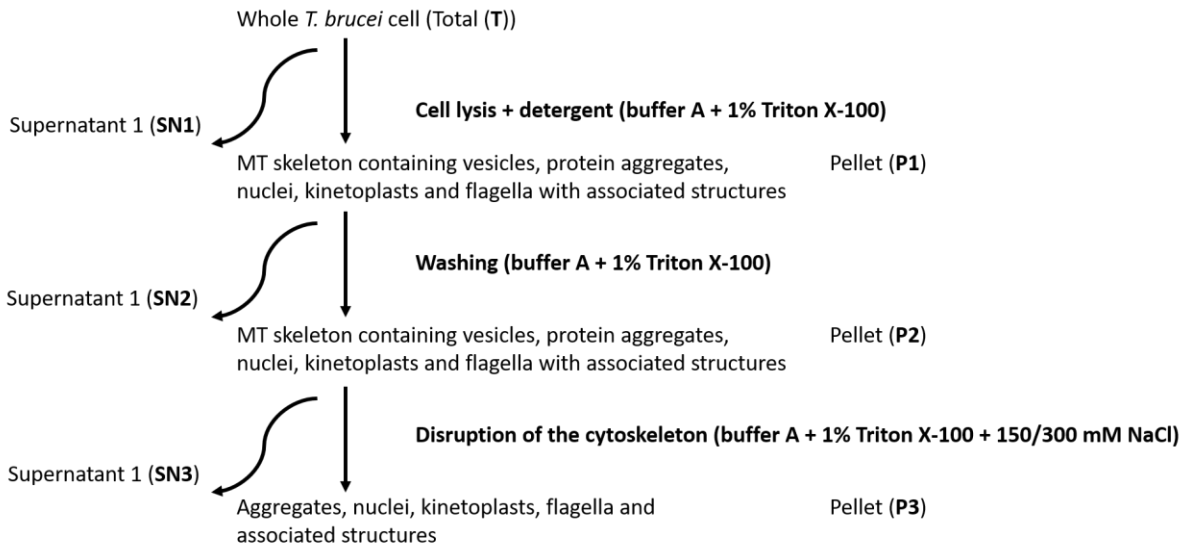

S1 Fig.: Schematic depiction of microtubule sieving technique. According to (32).

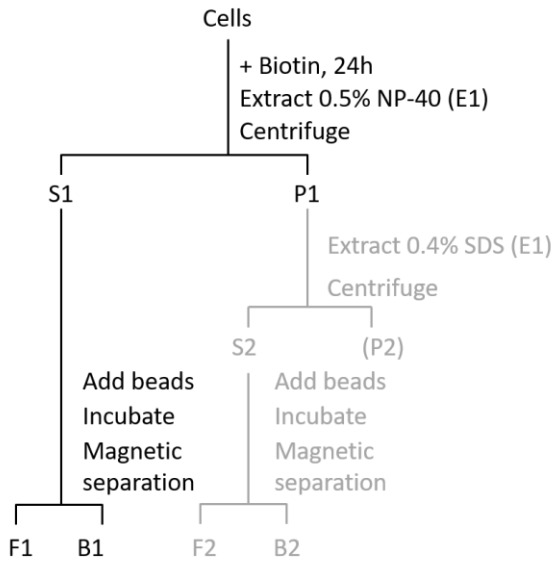

S2 Fig.: Schematic depiction of proximity-dependent biotinylation (BioID). According to (40). Only steps in black were performed in our study.

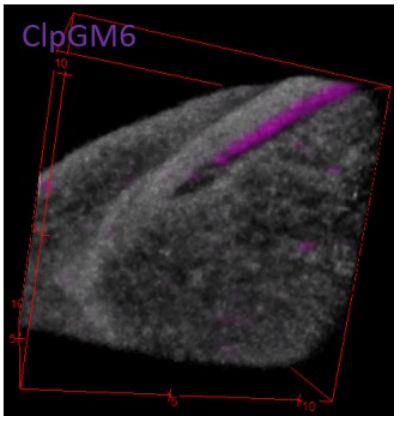

S3 Fig.: Ultrastructure expansion microscopy of a cell labelled with anti-ClpGM6 (to detect the FAZ, purple) and anti-tubulin antibody C3B9 (grey) to visualize the MT corset.

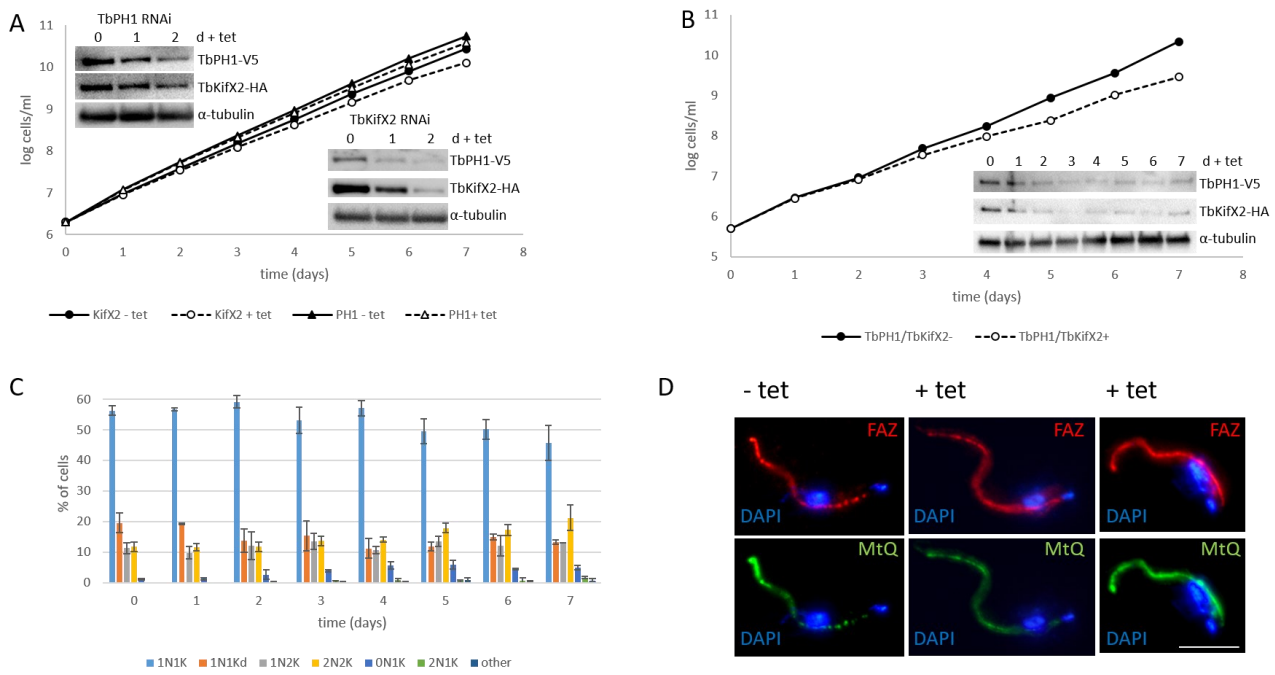

S4 Fig.: TbPH1/TbKifX2 RNAi. **(A)** Growth curves of TbPH1 and TbKIfX2 RNAi cell lines. Filled circles: TbKifX2 – tet, open circles: TbKIfX2 + tet, filled triangles: TbPH1 – tet, open triangles: TbPH1 + tet. Insets show western blots probed with anti-HA (to detect TbKifX2), anti-V5 (to detect TbPH1) and anti-α-tubulin as a loading control. **(B)** Growth curve of TbPH1/TbKifX2 RNAi cell line. Filled circles: TbPH1/TbKifX2 – tet, open circles: TbPH1/TbKifX2 + tet. Inset depicts western blot showing depletion of TbPH1/TbKifX2. Samples were taken at the same time as the growth curve in B was performed. The blot was probed with anti-HA (to detect TbKifX2), anti-V5 (to detect TbPH1) and anti-α-tubulin as a loading control. **(C)** Bar chart depicting different cell cycle phases during TbPH1/TbKifX2 RNAi time course. DAPI counts were performed in triplicate with at least 200 cells counted per time point. N: nucleus, K: kinetoplast. **(D)** IFA of TbPH1/TbKifX2 RNAi cells. + tet: induced for 5 days. Extracted cytoskeletons were labelled with L3B2 (recognising the FAZ filament, red), mAB 1B41 (recognising the MtQ, green) and DAPI. The scale bar corresponds to 5 µm.

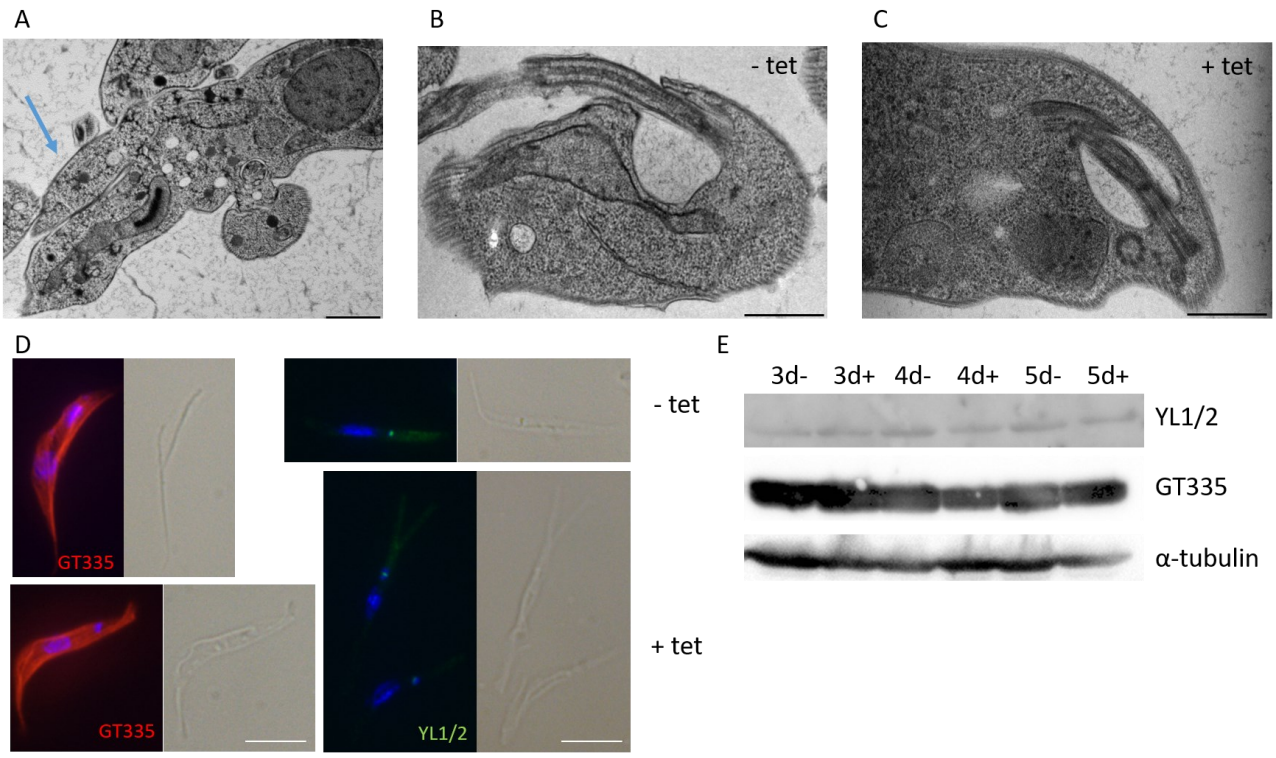

1119

1120 **S5 Fig.:** Transmission electron microscopy and IFA of TbPH1/TbKifX2 RNAi cell line. Cells were
1121 induced for 5 days. **(A)** Image depicting posterior end protrusions (arrow). The scale bar corresponds
1122 to 1 µm. **(B)** Flagellar pocket region of cells not induced for TbPH1/TbKifX2. The scale bar
1123 corresponds to 500 nm. **(C)** Flagellar pocket region of cells induced for TbPH1/TbKifX2 RNAi. The
1124 scale bar corresponds to 500 nm. **(D)** IFA on cytoskeletons probing effects of TbPH1/TbKifX2
1125 depletion post-translational modifications of tubulin. Cells were counterstained with GT335 (red,
1126 staining glutamyl side chains) and YL1/2 (green, staining tyrosinated α-tubulin). The scale bar
1127 corresponds to 5 µm. **(E)** Western blots taken after 3 to 5 days (d) of growth in presence (+) or
1128 absence (-) of doxycycline probed with antibodies recognizing GT335, YL1/2 and α-tubulin, the last
1129 as a loading control.

1130